Review article

Additively manufactured high-entropy alloys for hydrogen storage: Predictions

Morena S. Xaba

Advanced Materials Division, Mintek, Private Bag X 3015, Randburg, 2125, South Africa

A B S T R A C T

This review paper covers an analysis of the empirical calculations, additive manufacturing (AM) and hydrogen storage of refractory high-entropy alloys undertaken to determine the structural compositions, particularly focusing on their applicability in research and experimental settings. The inventors of multi-component high-entropy alloys (HEAs) calculated that trillions of materials could be manufactured from elements in the periodic table, estimating a vast number, N = 10^100, using Stirling's approximation. The significant contribution of semi-empirical parameters such as Gibbs free energy ΔG, enthalpy of mixing ΔH_{mix}, entropy of mixing ΔS_{mix}, atomic size difference $\Delta\delta$, valence electron concentration VEC, and electronegativity difference $\Delta\chi$ are to predict BCC and/or FCC phases in HEAs. Additive manufacturing facilitates the determination of refractory HEAs systems with the most stable solid-solution and single-phase, and their subsequent hydrogen storage capabilities. Hydride materials, especially those from HEAs manufactured by AM as bulk and solid materials, have great potential for H_2 storage, with storage capacities that can be as high as 1.81 wt% of H_2 adsorbed for a ZrTiVCrFeNi system. Furthermore, laser metal deposition (LMD) is the most commonly employed technique for fabricating refractory high-entropy alloys, surpassing other methods in usage, thus making it particularly suitable for H_2 storage.

1. Introduction

Traditional alloy composition normally consists of one principal element, and the other elements are often, in minor compositions to improve the physical and chemical properties for a desired application. About two decades ago, in year 2004, two groups of researchers, independently started manufacturing alloys of multi-component principal elements in equimolar ratios [1–4]. Their predictions were somehow, based on a general understanding of physical metallurgy and the facts concerning binary and ternary phase diagrams [5]. The base alloy method may be labeled as "matured technology", but this is only if no new materials can be produced from that technology that can bear materials with unprecedented properties to revolutionize human civilization [6]. Thus, multi-component principal alloys have taken the field of materials science and engineering to new level and indeed, they will be central to the field of structural, and perhaps functional materials in the next decades or longer. The current research direction is in the investigation of new high-entropy alloys (HEAs) and complex concentrated alloys (CCAs) that can operate with sustained strength at ever-increasing temperatures or the prospect of discovering new materials with unprecedented properties, or combinations thereof [7, 8]. In HEAs, each combination is a new alloy 'forms a base' because each HEA can easily be modified by addition of minor elements similar to traditional element-based alloy approach [9]. The abundance of novel alloy foundations stems from the numerous methods

by which primary elements can be selected from a palette of potential candidates. The formula delineating the quantity of distinct combinations of primary elements is given by equation (1) [6,9]:

$$C\binom{n}{r} = \frac{n!}{r!(n-r)!} \tag{1}$$

Here, *n* represents the count of elements available in the palette from which primary alloy components are chosen. With *n* being equal to 75 stable elements that are non-toxic, non-radioactive, and not noble gases, this yields more than 219 million potential CCA configurations featuring 3 to 6 primary elements. Hence, the importance of predicting the most stable solid-solution and single-phase HEAs become paramount, in order to reduce trials on experimental endeavors for specifically hydrogen storage applications.

Since the initial papers emerged in 2004, a discernible trend suggests that significant research interest in HEAs began around 2013, with researchers consistently keen on predicting the phases and microstructures of HEAs prior to experimentation [10]. There is also a limited composition space for HEAs due to material costs, resource availability, price stability, and recyclability [11]. So far, there are very few studies that have investigated the phase formation rules for multi-component HEAs, and this is because of the lack of information on phase diagrams for HEAs. As a result, high throughput screening tests and calculations are an essential part of the prediction strategy, and phase formation in HEAs remains a subject of investigation. One of the key opportunities is to expand the HEA scope and compositionally complex alloy design framework to include the work in the functional material class [6]. Fig. 1 depicts a publication trend from the Scopus database, for articles with "*high-entropy alloy*" and "*high-entropy alloy AND phase prediction*" from the year 2004–2024.

For articles published with the keyword "high-entropy alloy", only two articles in 2004 and steadily increased, in total to 3812 articles as of 2023, and the number is still increasing. This indicates the exponential growth and interest gained from researchers around the world for HEAs. In 2010, there was only one article published with the keyword "high-entropy alloy AND phase prediction" and in 2023, there were 187 articles. Again, it shows that researchers are now looking for ways to find phase-stable HEAs.

The 3d transition metals have been investigated extensively, and the refractory metals are studied for their high temperature and cryogenic applications. Other interstitial elements and metalloids such as carbon, aluminum, and nitrogen are studied to improve the mechanical and microstructural properties of the materials. Fig. 2 displays the primary elements currently utilized in the fabrication of HEAs.

Despite the costly nature of precious metals, certain noble metal HEAs have defied expectations by showcasing the capacity to form stable single-phase solid solutions, thereby offering a cost-effective alternative for advanced material applications [13]. These materials have garnered significant interest across various domains of applied research, including corrosion resistivity [14–20], micromechanical stability [12,20–25], and energy storage [26–28]. Their remarkable microstructural properties, influenced by crystallographic characteristics and thermodynamic factors, are attributed to the presence of intermetallic phases as well as face-centered cubic (FCC) or body-centered cubic (BCC) solid-solution phases [29–32].

2. HEAs phase predictions

Traditional alloys were historically favored for their simplicity, typically starting with a base element to which additional elements are added, forming alloys like aluminum (Al), cobalt (Co), nickel (Ni), titanium (Ti), and chromium (Cr) [33]. However, high-entropy
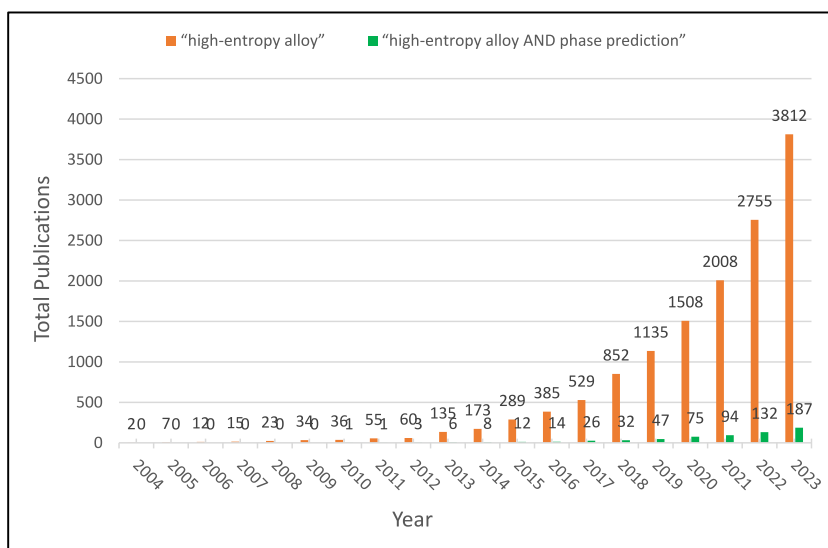

Fig. 1. Publication trend of articles with "*high-entropy alloy*" in orange bars and "*high-entropy alloy and phase prediction*" in green bars between 2004 and 2023. Data was obtained from the Scopus database.
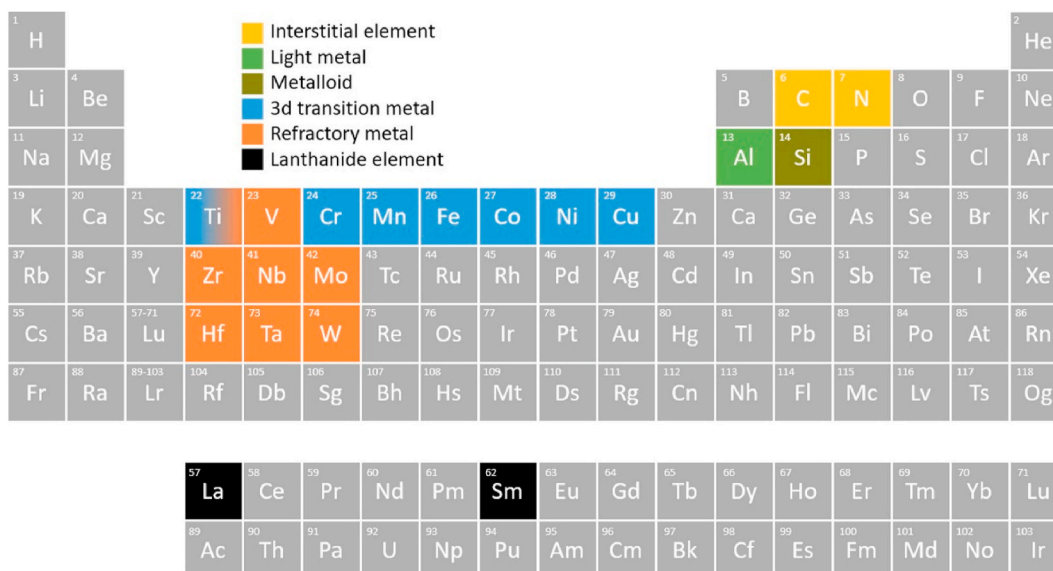
Fig. 2. Major elements used in the manufacturing of HEAs. Reproduced from Ref. [12].

alloys (HEAs) offer distinct advantages, possessing unique properties that traditional alloys may lack, prompting their adoption as they provide enhanced performance and functionality for various applications. The definition of HEA is still a subject of investigation; the two main known categories are based on composition and entropy. The composition-based definition is attributed to the presence of at least 5 different principal metallic elements in equiatomic or equimolar ratios, where the atomic percentage of each element in the alloy, varies from 5 % to 35 % [28,34]. The other minor elements that complete the HEA composition should have an overall percentage of less than 5 %. The entropy-based definition of HEAs is derived from blending or mixing, where the configurational entropy $\Delta S_{conf} > 1.5R$ and contains at least four elements, where R is the ideal-gas constant [22,28,35]. Furthermore, the impact of entropy is considerably more articulated in HEAs, it forms the backbone of the design and phase prediction. In thermodynamics analysis, the high-entropy effect determines the formation of complex, intermetallic, and single-phase alloys [36,37].

The design of every material or tool or device is always based on its intended potential end application. As a result, it will seem profitable to have guidelines for predicting, not only phases but other intrinsic application-oriented properties for HEAs [38–44]. The ability for materials to have desirable applications is normally investigated by characterizing a single dominant '*first-tier*' property, but sometimes multiple properties are required for certain applications [45,46]. In this respect, therefore, tensile properties will represent structural applications [21,23,32,47–52], magnetic saturation represents hard magnets [53,54], low-temperature conductivity will represent superconductors [55–57], and FCC phases will represent the H_2 storage domain [2,52,58–60]. It is well known that the prediction of the ability of solid-solution forming in HEAs remains a major challenge that hinders the discovery of novel HEAs. This review paper focuses solely on computational models utilizing semi-empirical methods, excluding coverage of machine learning applications. Scientists are presently advancing computational tools aimed at accurately predicting the desired properties of HEAs, representing an expanding area of research in materials science. Phase computations (PhaComp) methods is an example that is still under development in the United Kingdom, and it is showing promising results in the prediction of the formation of the *sigma* phases in CrMnCoFeNi$_x$ HEAs [61]. Researchers have been prompted to use computational methods to search easier, faster, and more accurately, as reported by Lederer et al., they proposed an *ab initio* simulation method and their results from the current most reliable data for binary, ternary, quaternary, and quinary systems were: 96.6 %; 90.7 %; 100 % and 100 %, respectively, of correct solid-solution predictions [62]. Other authors have used density functional theory (DFT) calculations to show that ΔS_{conf} in CrMoNbV stabilizes a single BCC phase from T = 1700 K up to melting, while precipitation of a complex intermetallic is favored at lower temperatures [44, 63]. The structure and elastic properties of the AlCrFeNiTi system were also predicted and calculated by using the DFT method [64]. Thermodynamics and kinetics fundamentals are quite very old and well-established methods, and they are also used in the prediction of the properties of HEAs [65–68]. High-entropy alloy predicting software (HEAPS), can be used to calculate the physical and semi-empirical parameters of alloys that are useful in predicting the phase and solid-solution formation ability of HEAs [69]. The calculations of phase diagrams (CALPHAD) method have also been shown to be useful for the calculation of phases and thermodynamic properties in HEAs systems [70–74]. A HEA with a nominal composition of FeCr$_{0.4}$V$_{0.3}$Ti$_{0.2}$Ni$_{1.3}$ was proposed based on the empirical thermodynamic models and CALPHAD calculations, and consistent with the prediction, the alloy consisted of dominant FCC phase and minor Ni$_3$Ti precipitates [75]. High-entropy alloys present a paradigm shift, offering unique properties that traditional alloys may lack, leading to their adoption across diverse fields. Computational models, including PhaComp and other emerging methods, hold promise in accurately forecasting properties crucial for HEA applications. Approaches such as *ab-initio* simulations and density functional theory (DFT) calculations demonstrate high accuracy in predicting solid-solution formation and phase stability. Additionally, established methods like thermodynamics and CALPHAD calculations contribute significantly to understanding and designing HEAs for

specific applications. As research in computational studies of HEAs continues to advance, it opens avenues for discovering novel alloys with tailored properties, shaping the future of materials science [76].

2.1. Empirical parameters

2.1.1. Thermodynamic consideration

The Hume-Rothery rules for solubility in binary alloys have been developed and extended to suitable applications for multi-component HEAs [77–88]. By the definition of Gibbs free energy (ΔG), when the temperature is sufficiently high, the entropy can stabilize the phase in question. Calculating ΔG for various compositions and temperatures of multi-component HEAs is challenging, but it was subsequently found that ΔG at a specific composition is proportional to the free energy of mixing ΔG_{mix} of the liquid phase as shown in equation (2) [85,89]. Now, the definition of the ΔG can be revised as follows [79,89,90]:

$$\Delta G_{mix} = \Delta H_{mix} - T \cdot \Delta S_{mix} \qquad (2)$$

where T is the absolute temperature, ΔH_{mix} is the enthalpy of mixing and ΔS_{mix} is the entropy of mixing. Therefore, if the enthalpy of mixing for a multi-component alloy system is adopted, the n-elements can be determined from equation (3) [64,69,80,89,91–93]:
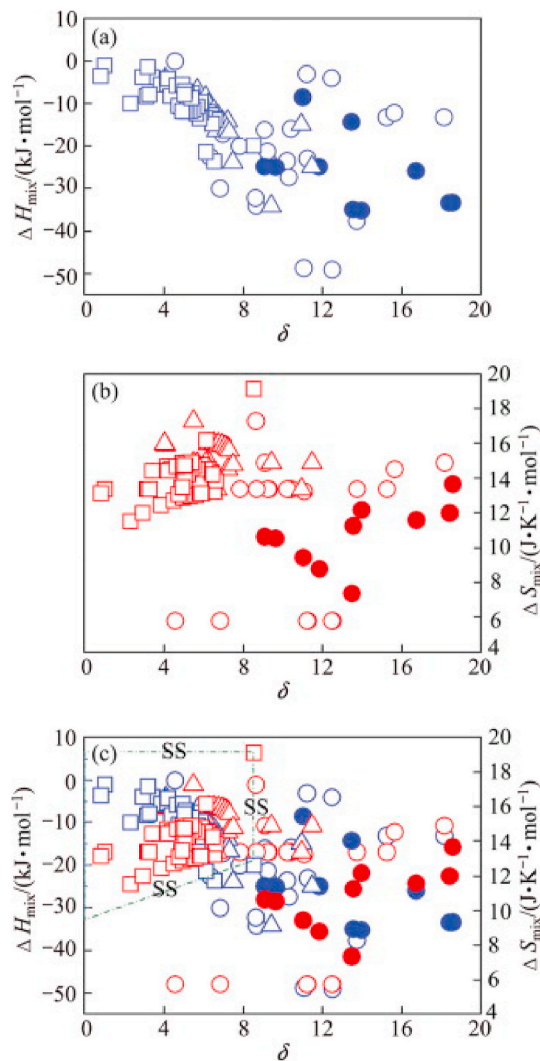
Fig. 3. Combined impact of ΔH_{mix} and δ (a), ΔS_{mix} and δ (b), and the collective influence of all three parameters ΔH_{mix}, δ, and ΔS_{mix} (c) on phase stability in equiatomic multi-component alloys. The symbol ○ represents equiatomic amorphous phase forming alloys; ● represents non-equiatomic amorphous phase forming alloys; □ represents solid solution phases and △ represents intermetallic phases. Reproduced from Ref. [96].

$$\Delta H_{mix} = \sum_{i=1,i\neq j}^{n} \Omega_{ij} \cdot C_i \cdot C_j \tag{3}$$

where $\Omega_{ij} = 4 \Delta H_{AB}^{mix}$ is the regular solution interaction parameter between the ith and jth elements, C_i or C_j are the atomic percentages of the ith or jth components, and ΔH_{AB}^{mix} is the enthalpy of the mixing of binary liquid alloys. According to Boltzmann's hypothesis, the entropy of mixing the n-element regular solutions is given by equation (4) [69,80,92,93]:

$$\Delta S_{mix} = -R \sum_{i=1}^{n} (C_i \cdot Ln C_i) \tag{4}$$

where C_i is the mole percent of component $\sum_{i=1}^{n} (C_i) = 1$, and $R = 8.314$ JK^{-1}mol^{-1} is the gas constant. Therefore, the high mixing entropy reduces the free energy of the solid-solution phase and promotes the formation of solid-solution at higher temperatures. The number of phases of HEAs decreases because of the enhancement in the mutual solubility between the elements [94]. The effect of a high entropy was proposed by one of the authors who first invented HEAs, and they assumed that the composition of equiatomic alloys may form intermetallic phases [3]. This understanding allows for revising ΔG definition, incorporating enthalpy (ΔH_{mix}) and entropy (ΔS_{mix}) of mixing, facilitating determination of n-elements in multi-component alloy systems. High mixing entropy reduces free energy, promoting solid-solution formation at elevated temperatures, thereby reducing the number of phases in HEAs and enhancing mutual solubility between elements. This concept, proposed by HEA inventors, underscores the potential of equiatomic alloys to form intermetallic phases.

2.1.2. Atomic size difference

Atomic size difference ($\Delta\delta$), plays a crucial role in determining the stability and phase formation of HEAs, expressed as a weighted average of atomic radii, it also governs the formation of simple phases such as BCC and FCC. Therefore, to describe the comprehensive effect of the atomic size difference in an n-element alloy, the parameter $\Delta\delta$ is expressed in equation (5) as follows [69,92,93,95]:

$$\Delta\delta = \sqrt{\sum_{i=1}^{n} C_i \cdot \left(1 - \frac{r_i}{\bar{r}}\right)^2} \tag{5}$$

where C_i is the atomic percentage of the ith component, $\bar{r} = \sum_{i=1}^{n} C_i r_i$, where r is commonly taken to be the Goldschmidt atomic radius of element i and $\bar{r}$ is the weighted average of the system's atomic radii [69,80,89,92,93]. The sole simple phases BCC, FCC, and their mixtures, need to simultaneously satisfy the following conditions: $-22 \leq \Delta H_{mix} \leq 7$ kJ mol^{-1}, $\Delta\delta \leq 8.5$, and $11 \leq \Delta S_{mix} \leq 19.5$ JK^{-1}mol^{-1} [79,93,96,97] to be formed. More importantly, a small value of $\Delta\delta$ indicates a high possibility for the formation of a single-phase solid solution, and a large value of $\Delta\delta$ suggests the formation of an amorphous phase and multi-phases in HEAs [79,98,99]. As demonstrated in Fig. 3a, ΔH_{mix} cannot be too large in value because a large positive ΔH_{mix} leads to phase separation and a large negative ΔH_{mix} leads to intermetallic phases. The region delineated by the dash-dotted lines in Fig. 3c indicates the requirements for solid solution phases to form.

Atomic size difference needs to be small enough since large $\Delta\delta$ leads to excess strain energy and destabilizes simple structures. Entropy of mixing ΔS_{mix} must be large enough because it is the main stabilizing factor for simple phases. Zhang et al. [79], proposed that small atomic size differences and near-zero values of the absolute enthalpy of mixing facilitate the formation of solid solutions for multi-component alloys, i.e., the $\Delta\delta$ should be less than 6.5 %, the ΔH_{mix} should be in the range of between -15 to 5 kJ mol^{-1}, Fig. 3a,
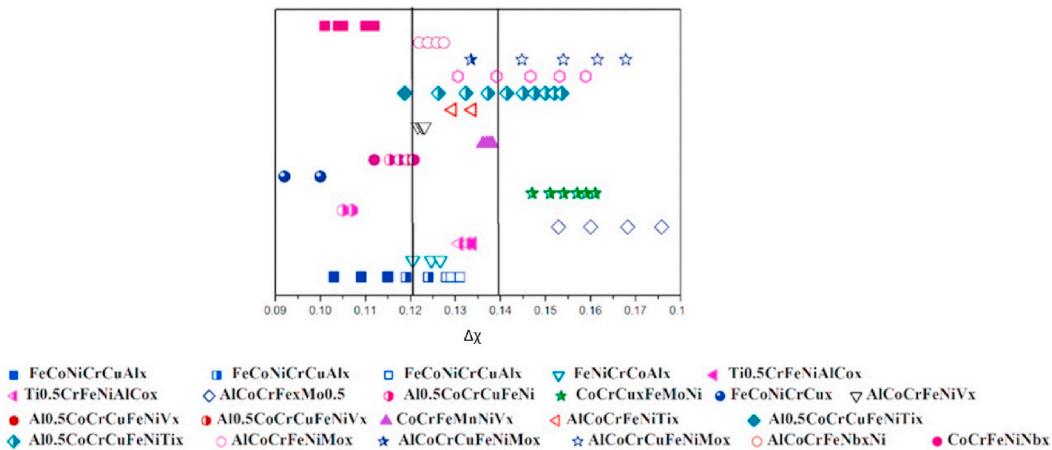

Fig. 4. Influence of $\Delta\chi$ on the HEAs phases, note on the legend: fully closed symbols for sole FCC phases; fully open symbols for sole BCC phase; half closed symbols for mixes FCC and BCC phases. Reproduced from Ref. [101].

and the ΔS_{mix} should be in the range of between 12 and 17.5 J K^{-1} mol^{-1}, Fig. 3b. Small $\Delta\delta$ favors single-phase solid solutions, while large $\Delta\delta$ leads to amorphous or multi-phase formations. Additionally, ΔH_{mix} and ΔS_{mix} must be within specific ranges for solid solution formation.

2.1.3. Electronegativity difference

Considering that different elements have different numbers of electrons and protons in their nucleus, it is important to examine the influence of electronegativity difference ($\Delta\chi$) in the phase formation rules for HEAs. The electronegativity difference, $\Delta\chi$ in equation (6) can be calculated from the Pauling electronegativity of elements in an alloy by the following expression [64,77,96,99,100]:

$$\Delta\chi = \sqrt{\sum_{i=1}^{n} C_i \cdot (\chi_i - \overline{\chi})^2}, \overline{\chi} = \sum_{i=1}^{n} C_i \cdot \chi_i \tag{6}$$

where n is the number of components, C_i is the concentration of component i, χ_i is the Pauling electronegativity of component i and $\overline{\chi}$ is the average electronegativity of the n components in the alloy. Fig. 4 shows the $\Delta\chi$ variation for different compositions. The distribution of $\Delta\chi$ for different compositions exhibits that for $\Delta\chi \geq 0.138$, the FCC phase was not stable whereas for $\Delta\chi \leq 0.115$, the FCC and FCC + BCC phases were stable [101].

2.1.4. Valence electron concentration

The other parameter that controls the specific phase formation in HEAs is the valence electron concentration (*VEC*) equation (7), and it is described as a weighted average of the valence electrons of the constituent elements [31,64,77,96]:

$$VEC = \sum_{i=1}^{n} C_i \cdot VEC_i \tag{7}$$

where n is the number of components, C_i is the concentration of component i and VEC_i is the valance electron concentration of component i. The *VEC* was found to be the physical parameter to control the phase stability for FCC or BCC solid solutions. FCC phases were found to be stable at higher $VEC \geq 8$, and BCC phases were stable at low $VEC < 6.87$ [31,64,99]. To illustrate this concept, Chen et al. investigated the balance between strength and ductility of CoCrCuFeNi and AlCoCrFeNi HEAs, providing insights into their mechanical behavior and potential applications in structural materials [102]. Their observations revealed a notable enhancement in compressive fracture strain, rising by 15 %, as the nickel concentration escalated from 0 atomic percent to 16 atomic percent. Concomitantly, the VEC exhibited an uptick from 7.2 to 7.6, coinciding with a transition in phases from BCC to FCC, as depicted in Fig. 5a. As the molybdenum concentration surged from 0 atomic percent to 16 atomic percent, a substantial augmentation of 668 MPa was noted in the compressive yield strength. This increase was accompanied by a decrease in the VEC from 8.8 to 8.3, coinciding with a shift in phases from FCC to BCC, as illustrated in Fig. 5b.

2.1.5. Chemical bond mismatch

Ignoring the solid-state phase transition, the phase formation generally occurs near the melting temperature (T_m) of an alloy. Hence, the T_m is adopted for the entropy term, $T\Delta S_{mix}$, and a parameter Ω is defined for predicting the solid-solution formation for various multi-component alloys as exemplified in equation (8) below [69,80,92,93,96]:

$$\Omega = \frac{T_m \cdot \Delta S_{mix}}{|\Delta H_{mix}|} \tag{8}$$
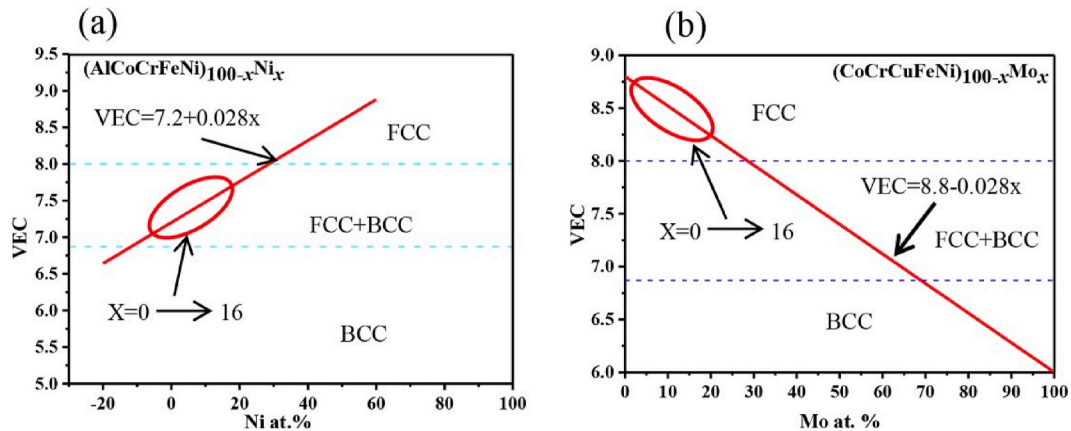

Fig. 5. Valence electron concentration in terms of the i-th component concentration C_i for the HEA systems (a) (AlCoCrFeNi)$_{100-x}$Ni$_x$ and the (b) (CoCrCuFeNi)$_{100-x}$Mo$_x$. Reproduced from Ref. [102].

The melting point temperature of n-elements alloy, T_m, is calculated by using the rule of mixtures and it is expressed by equation (9) [69,80,89,92,93]:

$$T_m = \sum_{i=1}^{n} C_i \cdot (T_m)_i \tag{9}$$

Here, $(T_m)_i$ is the melting point temperature of the ith component of the alloy. As analyzed above, the value of Ω is positive, and when $\Omega = 1$ should be proposed as a critical value to form the solid solution. If $\Omega > 1$, the contribution of $T\Delta S_{mix}$ will exceed that of ΔH_{mix} for a solid-solution formation, and the multi-component HEAs are mainly composed of the solid solutions; if $\Omega \leq 1$, ΔH_{mix} is the predominant part of the free energy, and intermetallic compounds and segregations before solid-solution phases to form in multi-component HEAs. Thus, the value of Ω is used to estimate the solid-solution formation ability.

Yang and Zhang calculated the value of Ω and δ various other HEAs to find the relationship for determining the formation of solid solutions, intermetallic, solid solutions plus intermetallic, and amorphous compounds [80]. Through their calculation of Ω and δ from the collection of data from other authors who experimentally manufactured the HEAs, the phase comparison showed that; for an alloy to be in a solid-solution it must have a value $\Omega \geq 1.1$, as well as the value $\delta \leq 6.6\%$, as shown in Fig. 6. From Fig. 6, one could categorize that the solid solution phase can be formed only when the atomic size difference is small enough and Ω has a large value. According to equation (8), if the value of ΔS_{mix} is large enough to exceed that of $|\Delta H_{mix}|$, the strain caused by lattice distortion is lower in the HEA and, therefore the possibility of finding HEAs with a single phase will be high [80].

Phase formation in alloys typically occurs near their melting temperature (T_m). The T_m is utilized in the entropy term, $T\Delta S_{mix}$, with a parameter Ω defined to predict solid-solution formation in multi-component alloys. Ω, calculated as $(T_m \cdot \Delta S_{mix})/(|\Delta H_{mix}|)$, determines whether solid solutions form predominantly or intermetallic compounds and segregations occur. $\Omega > 1$ signifies solid-solution dominance, while $\Omega \leq 1$ indicates intermetallic compound formation. Larger Ω values and smaller atomic size differences favor solid-solution formation. High ΔS_{mix} relative to $|\Delta H_{mix}|$ reduces lattice strain, increasing the likelihood of single-phase HEAs.

3. Core HEA effects

High Entropy Alloys exhibit unique properties attributed to four core effects: the high-entropy effect, lattice distortion effect, sluggish diffusion, and the 'cocktail' effect. These effects collectively contribute to the remarkable performance of HEAs in various applications. The high-entropy effect arises from the simultaneous presence of multiple elements in equiatomic or near-equiatomic proportions, leading to a highly random atomic arrangement and increased configurational entropy [103]. This effect enhances the stability of solid solutions and suppresses phase transformations. The lattice distortion effect refers to the distortion of the crystal lattice caused by the presence of different-sized atoms, which impede dislocation movement and enhance mechanical properties. Sluggish diffusion, resulting from the complex atomic configurations in HEAs, retards diffusion processes, contributing to high-temperature stability and resistance to phase separation. Lastly, the 'cocktail' effect describes the synergistic interactions between alloying elements, leading to emergent properties not present in individual constituent elements. These effects collectively define the unique behavior and performance of HEAs, making them promising candidates for advanced engineering applications. Additionally, they can assist in crafting materials when exploring novel compositions or applying them in various contexts.

3.1. High-entropy effect

One of the signature concepts of HEAs is that the configurational entropy can be used to control microstructure, for example, solid solutions, and phases with simple structures FCC, BCC, and hexagonal close-packed (HCP) [77]. When the alloy has an equiatomic ratio with 5 or more components, the solid-solution is highly favored over the competing intermetallic compounds. The
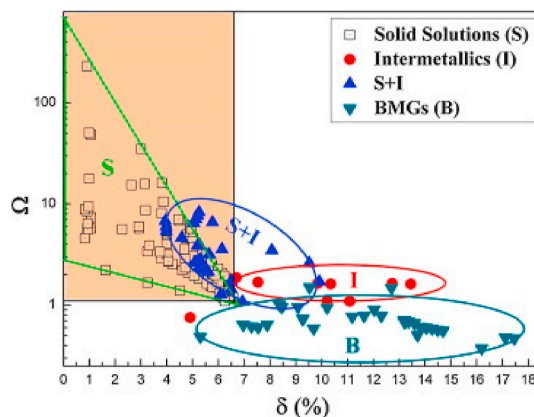

Fig. 6. Parameter values of Ω *vs.* δ for various HEAs. Reproduced from Ref. [80].

configurational entropy or mixing entropy in HEAs, lowers the free energy at high temperatures and the mutual solubility among constituent elements, allows for reduced phases to be formed [104,105]. However, it should be emphasized that the high-entropy effect does not 'guarantee' the formation of simple solid solution phases, BCC, or FCC at high temperatures; it merely reduces the possibility of a multiple-phase formation [99]. In addition, in the Gibbs free energy, entropy can stabilize a phase with high entropy provided the temperature is high enough. The mixing entropy of an equimolar quinary random solid-solution is $1.6R$, this means that the entropy difference between an equimolar quinary solution and a completely ordered phase is about 60 % larger than the entropy difference between liquid and solid states of pure metals [77,81,99]. Kube & Schroers suggested that the HEAs form metastable single-phase solid solutions through polymorphic solidification, upon rapid cooling [94]. In their assessment, they proposed that the corresponding critical cooling rate of single-phase solid solutions formation is a quantitative measure that characterizes the degree of single-phase solid solutions metastability and forming ability of HEAs. For single-phase HEAs, the determination of the compositional and thermal stability regions with excellent properties and the potential for engineering applications is still a subject of investigation.

3.2. Lattice distortion effect

The severe lattice distortion caused by unequal sizes of atoms that make up the crystal lattices affects the local environment of the HEAs [106]. Larger atoms push away their neighbors and their smaller counterparts have extra space around them. The strain energy associated with lattice distortion raises the overall free energy of the HEA lattice [99]. These distortions contribute to the configurational entropy of HEAs, and they are also believed to decrease the intensity of the *X*-ray diffraction peaks, and other properties such as hardness, electrical and thermal conductivity, and temperature dependence [9,78,107,108]. However, there are still some missing systematic quantification results that must support these claims to set them apart from other external factors, *e.g.*, the direct measurement of the degree of lattice distortion/strain [109,110]. Continued research into lattice distortions in HEAs holds promise for unlocking their full potential. Systematic quantification will enhance understanding and distinguish their effects from other factors, advancing the development of advanced materials.

3.3. Sluggish diffusion effect

The diffusion and phase transformation kinetics in HEAs are considerably slower than in traditional alloys [77,111]. The ability for atoms to migrate back and forth in a lattice structure is dependent on the energy of that vacant site where the atom is located. This means that when the energy of the vacant site is lower than where it came from then that atom may be trapped on that new site, and inversely if the site has high energy, then that atom may migrate back to its original place as demonstrated by Tsai et al. [112]. Fig. 7 shows this in pictographic form, for pure elements, the energy potential difference for an atom moving from one place to another is zero, but, for HEAs, the energy potential is high.

Another factor responsible for sluggish diffusion is that the diffusion of each atom in the HEA system is different. For example, high melting point elements, and these elements now compete with others and the success rate here determines the solid solution phases [99]. The sluggish diffusion and phase transformation kinetics in HEAs, compared to traditional alloys, highlight the unique challenges and opportunities in their design and application. This observation underscores the need for further exploration to optimize their performance and unlock their full potential.
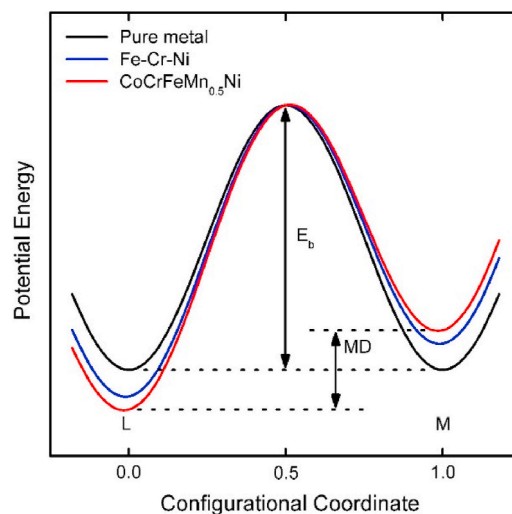
Fig. 7. Potential energy difference in the migration of a Ni atom, the mean difference in potential energy before (blue line) and after (red line) migration. Reproduced from Ref. [112].

3.4. Cocktail effects

Like in any newly invented system, there are unexpected interactions between the individual components. In low-density elements, e.g., aluminum, this can lead to light metals HEAs, and for elements with high melting temperatures e.g., zirconium, this can lead to refractory metal HEAs. With the hexagonal close-packed crystal structure, this can lead to single-phase HEAs [77]. Unlike the other three core effects, the cocktail effect cannot be measured and characterized since it is used to describe the many possibilities and unknown expectations from the synthesis of HEAs [113]. The exploration of High Entropy Alloys (HEAs) unveils unexpected interactions among their constituent elements, yielding diverse outcomes such as light metals or refractory metal HEAs. The cocktail effect, representing these varied possibilities, underscores the complexity of HEA synthesis and the need for comprehensive investigation.

4. Additive manufacturing of HEAs

Unlike conventional subtractive manufacturing methods, additive manufacturing (AM) is based on a layer-by-layer addition of materials on top of each other to produce a product [114,115]. This could be achieved by either melting the material, sintering or by applying pressure. As such, metal AM technologies commonly use powder or wire as feedstock that is selectively heated and melted followed by consolidated cooling to form a part [116]. AM techniques date back four decades; however, their applications were limited to the rapid manufacturing of porous structures and prototypes. Today, AM is attracting much attention due to its advantages such as design freedom and short lead times [117]. As the know-how of the technology progresses, the resulting microstructure and properties of the manufactured parts become more prevalent for industrial applications [118,119]. Many researchers have worked on inventing new alloys that could be highly sophisticated, especially for materials engineering applications. The HEAs produced by the induction melting or vacuum arc melting method require repeated re-melting to achieve the necessary chemical homogeneity and this causes significant phase separation [49,120–124]. The use of metal additive manufacturing, more importantly, direct metal deposition in the class of high-entropy alloys, allows for fast cooling and solidification rates and enables the production of fine crystallographic complexes [37,119,125,126]. Dobbelstein et al., successfully demonstrated that direct metal deposition can be used to produce refractory HEAs, from a mixture of elemental powders through *in-situ* alloying with improved mechanical strength at elevated temperatures [127, 128]. To achieve a high relative density, typically >99.5 %, researchers have focused their attention on the transition element process parameters optimization and control to avoid crack propagation and poor mechanical performance, and subsequently the phase rearrangement [12,116,129]. This section of the review will focus on the manufacture of HEAs from 3 a.m. techniques, namely; selective laser melting (SLM), electron beam melting (EBM), and laser metal deposition (LMD) as illustrated in Fig. 8.

Despite their varying processing steps, they all share the same approach, *i.e.*, a 3D CAD file is the starting point in which the machine converts its sliced model into thin layers with a typical layer thickness of between 20 μm–1 mm [116,119]. In the SLM technique, metal powder is spread across the work area or substrate in a layer thickness of between 20 μm–100 μm. The metal powder is then fed by a hopper or coater to provide a uniform distribution of the powder layer [133]. A laser beam with a fixed laser power is directed to the deposited powder layer at a specific scanning rate, the powder layer is melted, and it solidifies to form a part Fig. 8b. LMD parts are created by applying a metal powder to the work area and simultaneously melting it to form the part. The metal powder is fed by a coaxial or multi-jet nozzle, while the melt pool is protected from oxidation by a continuous supply of an inert gas such as argon or helium Fig. 8a [130]. The metal powder in EBM is spread similarly to the SLM process Fig. 8c, however, instead of a laser beam, an
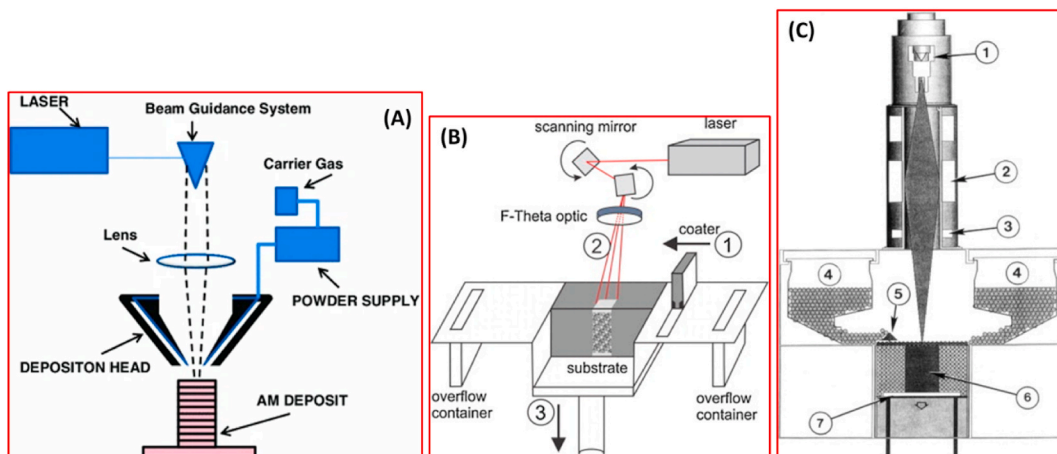
Fig. 8. Representation of the working principle of the three metal additive manufacturing categories with main terminology. **(a)** Schematics of an LMD set-up. Reproduced from Ref. [130]. **(b)** Schematic of SLM, labels; 1 = powder layer coater, 2 = laser beam, 3 = print bed. Reproduced from Ref. [131]. **(c)** Schematic of EBM, labels; 1 = electron gun, 2 = lens system, 3 = deflection lens, 4 = powder cassettes with feedstock, 5 = roller or rake, 6 = building component, 7 = print bed. Reproduced from Ref. [132].

electron beam is used to melt the metal powder into a solid part [132,134].

4.1. HEAs via selective laser melting

Selective laser melting (SLM) is an additive manufacturing technique that uses a high-energy laser beam to selectively fuse powdered materials, layer by layer, to produce intricate and customized three-dimensional parts. This innovative method offers precise control over material composition and microstructure, making it ideal for fabricating complex geometries with superior mechanical properties. A bulk nanostructured equimolar $A\ell$CoCrFeMnNi system was fabricated using the SLM technique and consisted of $A\ell$ & Ni-rich ordered and Cr & Fe-rich disordered BCC phases [135]. The high-energy laser beam of the SLM process caused Mn inhomogeneity due to partial evaporation, and due to rapid cooling rates, the formation of coarse columnar grains elongated in the built direction was observed. The other parameter playing a significant role in the microstructure of the HEAs is the annealing temperature. The evolution of dislocation networks which is a unique structure that results from rapid solidification affects the microstructural properties of the material [136–138]. The CoCrFeNi was composed of a single-FCC solid-solution, and the residual stress and microhardness decreased with an increase in annealing temperature. Chen et al. decided to blend pre-alloyed CoCrFeNi powder and elemental Mn powder, to form quasi-equiatomic CoCrFeMnNi by SLM process [139]. Though the material consisted of FCC + Mn_2O_3 phase, it had high tensile strength, and compression ductility, but a moderate tensile ductility. The Mn_2O_3 phase resulted from the remelting of the oxide surface of elemental Mn powder as shown in Fig. 9.

By increasing the $A\ell$ composition in $A\ell_x$CrCuFeNi$_2$ produced by SLM, resulted in cracking and changes in the microstructure of the material. With an increase in the $A\ell$ content, there existed a transition of crystalline structures from FCC to FCC + BCC/B2 [51,140]. It is recommended that the composition of double the Ni content in this system should be lowered to the other elements, and only vary the $A\ell$, to better understand the true nature and cause of the cracking behavior.

4.2. HEAs via laser metal deposition

Laser metal deposition (LMD) is an additive manufacturing technique where a focused laser beam melts metal powder or wire as it is deposited onto a substrate. This method enables precise control over material deposition, making it suitable for repairing, coating, or fabricating complex, near-net-shape components with tailored properties [141]. Manufacturing techniques using lasers are methods used in surface engineering and are multi-faceted techniques that contain lasers, optics-guided systems, and carrier gases and are operated in an inert atmosphere [142–145]. HEAs were manufactured through the LMD system to create fully, equiaxed grain microstructures in $A\ell$CoCrFeNiTi$_{0.5}$ alloy [146]. It was found that the increase in the laser traverse speed or the decrease of the laser power led to a larger temperature gradient. One of the advantages of the LMD technique is the ability to vary these parameters thus, allowing for the investigation of the microstructures and mechanical properties of the HEAs [16,23,48,120,147]. Kinetic effects play a considerable role in the phase stability of HEAs, especially during the formation of intermetallic phases in multi-component alloys. This simply suggests that phase selection in HEAs can be tailored by controlling the kinetic factors during fabrication. As a result, the investigation of the influence of laser parameters is important for the prediction of the basic microstructure and properties of HEAs [15, 148–151].

Kunce et al. reported on the ZrTiVCrFeNi, LaNiFeVMn, and TiZrNbMoV alloys, fabricated with the LMD method, which were studied for their elemental compositions in the alloy phases and the hydrogen absorption–desorption properties associated with them [2,52,152]. Based on their results, ZrTiVCrFeNi, with a dominant C14 Laves phase, showed a maximum hydrogen capacity of 1.8 wt% and 1.56 wt% at 100 bar and 50 °C for the as-synthesized and annealed samples, respectively [2]. TiZrNbMoV alloy manufactured with different laser power led to different phase compositions and hydrogen storage capacities [52]. The multiphase alloys with a mixture of
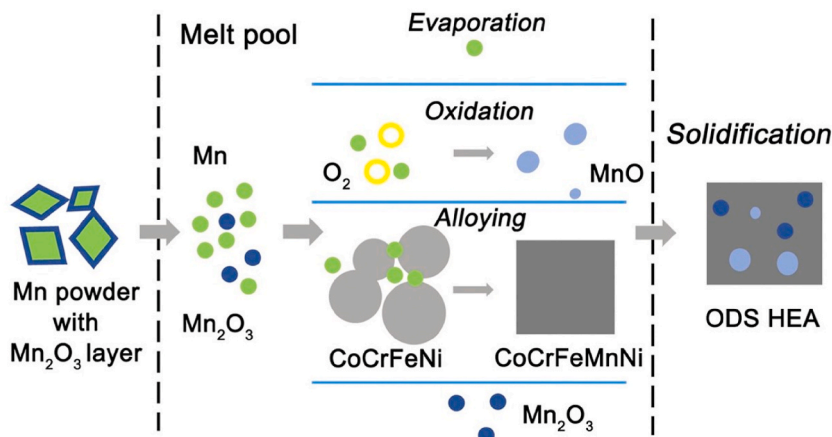

Fig. 9. Schematic illustration of an *in-situ* reaction of the Mn elemental powder to form MnO and Mn_2O_3. Reproduced from Ref. [139].

BCC solid-solution and intermetallic Laves phase were found to have the intermediate properties of high hydrogen storage and fast kinetics. A maximum hydrogen capacity of 1.18 wt% and a reversible phase transformation, from BCC to FCC, during the hydrogenation process at room temperature and atmospheric pressure for the TiZrHfMoNb alloy, was also reported [153].

4.3. HEAs via electron beam melting

Electron beam melting (EBM) is an additive manufacturing process that utilizes an electron beam to selectively melt and fuse metal powder particles layer by layer. This method offers high precision and can produce fully dense, complex parts with excellent mechanical properties, making it valuable in aerospace and medical applications. In 2015, Fujieda et al. were the first to show that AℓCoCrFeNi can be successfully manufactured by a selective EBM process [154]. They discovered the relationship between mechanical and microstructure properties, and specifically that the fracture strength was six times higher than the material manufactured by the conventional casting method [154,155]. By using the phase maps, they identified the existence of the BCC + FCC phases, however, they also observed that the abundance ratio of the FCC crystals in the bottom part, was about three times higher than that in the top part of the built column, as shown in Fig. 10.

They attributed the results to the longer preheating processes, which caused the phase transformations from BCC to FCC as it cooled. It will be interesting to observe the phase evolution by *in-situ* annealing during the electron beam melting process, which has never been reported to date. The corrosion behavior of the AℓCoCrFeNi was investigated for potentiodynamic polarisation in a 3.5 wt % NaCℓ solution and the results revealed that the product manufactured by the EBM process showed better corrosion performance than the material prepared by the conventional vacuum arc-melting method [156,157]. The obtained materials comprised of BCC, B2, and FCC phases, and the electrochemical properties of the EBM products were influenced by the phase morphologies formed during the pre-heating process [158].

The manufacturing of Aℓ$_{0.5}$CrMoNbTa$_{0.5}$ by the selective EBM process was demonstrated, however, it was not possible to achieve a completely homogeneous microstructure [159]. In this case, the process parameter optimization, rather than just post-process heat treatment, should be performed to reduce the porosity of the material. AℓCoCuFeNi consisting of a BCC solid-solution matrix with uniformly dispersed FCC-structured precipitates were fabricated by this procedure [160]. Furthermore, using the EBM during the electron beam melting process could result in a high relative density, finer microstructure, *in-situ* strengthening, and enhanced compressive properties.

Refractory WMoTaNbTi alloy produced by EBM with negative defocus distance was investigated [161]. The process resulted in the vaporization of Nb and Ti elements during the formation of HEA, however, the single BCC phase remained stable. The mechanical and microstructure behavior of the product formed at a scanning speed of 2.5 ms^{-1}, however, exhibited high strength. The authors also used the data from Takeuchi et al. [162], to calculate the atomic size difference $\Delta\delta$, concerning the scanning speed and predicted that a
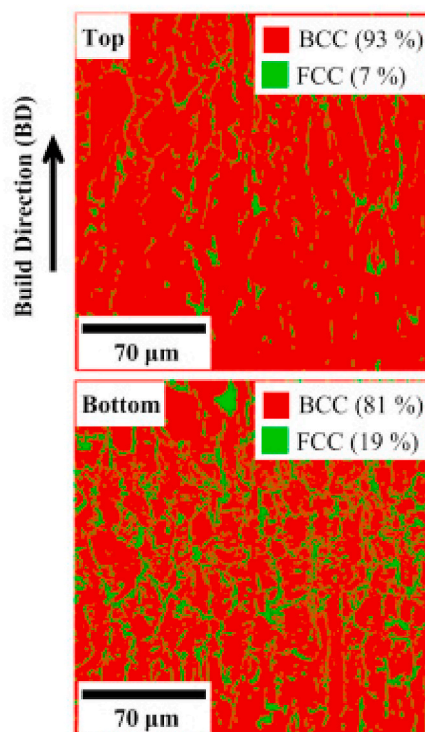

Fig. 10. Phase maps of the top part and the bottom part of the AℓCoCrFeNi manufactured by a selective EBM process. Reproduced from Ref. [154].

solid solution could be formed [161]. Carbon at 0.5 wt% in the form of graphite was incorporated to decrease the cracking behavior in WMoTaNbC refractory high-entropy alloy [163], and the results revealed the fact that carbon was responsible for the prolonged so-lidification ranges and the eutectic reaction into WMoTaNb, which caused the formation of dense dendrites and thus, lowered the cracking susceptibility. In another study, WMoTaNbV alloying powder was physically mixed with FeCoCrNi alloying powder, and the final mixture was additively manufactured by selective EBM. The as-deposited WMoTaNbVFeCoCrNi showed significant elemental segregation that consisted of multiple phases, including BCC, FCC, and the Laves phases [164]. In comparing various additive manufacturing methods for HEAs, each technique offers unique advantages and challenges. SLM provides precise control over material composition and microstructure, ideal for producing intricate parts with superior mechanical properties. EBM offers high precision and fully dense parts, critical applications, which is also expensive. LMD enables repairs, coatings, and near-net-shape fabrication with tailored properties.

5. Hydrogen storage properties of AM HEAs

Hydrogen is a useful source of energy, and its production and storage have been a subject of intense investigation for many decades. Hydrogen is still by far, the most valuable source of renewable and sustainable solutions for the reduction of the worldwide con-sumption of fossil fuel. The bottleneck of this green source of fuel is its storage, hence it is still a matter of ongoing investigation [165–167]. In this section, we will concentrate on H_2 absorption and desorption both before and after activation, examine the impact of temperature on H_2 absorption, and finally, evaluate the recyclability of the HEA material. Developing alloys that can rapidly and efficiently hydrogenate and dehydrogenate at room temperature, have high-volume density is a significant challenge for achieving safe and compact hydrogen storage [168,169]. Metal hydrides are able to store hydrogen due to their intermetallic phases that exist in BCC and FCC, and their rich C14 Laves phases [58]. HEAs are gaining attention for their potential in various applications due to their exceptional properties and distinctive microstructures, promising advancements in materials science and engineering. The latest approach to adjusting the thermodynamic stability of hydrides for hydrogen storage involves the use of multi-component high-entropy hydrides derived from HEAs, as illustrated schematically in Fig. 11.

When hydrogen is absorbed, it forms hydrides within the HEA matrix. The equilibrium plateau pressure (P_{eq}) is a key parameter indicating the pressure at which hydrogen uptake and release occur at a given temperature [171]. Proper tuning of P_{eq} in HEA hydrides ensures efficient hydrogen absorption and desorption at practical temperatures and pressures, making them ideal for storage appli-cations. High entropy alloys also possess a configurational entropy that is $\Delta S_{conf} \geq 1.5R$, and due to this fact, their crystal distortions are unique, and this gives an advantage to the phases that exist for hydrogen storage [104]. HEAs with a single-phase BCC structure are reported to be high-capacity metallic alloys for hydrogen storage purposes [37,172–174]. The BCC and Laves phase alloys exhibit high reactivity with hydrogen at room temperature, and these alloys are promising hydrogen storage future materials [175,176]. The high-entropy effect promotes the formation of a single C14 Laves phase, and the maximum H_2 storage capacity is closely correlated with the formation enthalpy of H_2 and the alloy. Hence, multicomponent HEAs with BCC and Laves phases offer numerous oppor-tunities for superior H_2 storage in practical applications. It was apparent that the elements in the alloy, played different roles, based on their covalent bonding energies with hydrogen atoms during hydrogenation [177]. Therefore, it is also important to optimize the fabrication steps of HEAs for an enhanced hydrogen storage capability, as demonstrated by other studies [123,178]. HEAs containing *ca.* 95 wt% of stable C14 Laves structure are highly desirable in an alloy for hydrogen storage applications [177,179,180].

Given that experimental measurements of hydrogen storage properties are extremely time-consuming, computational tools are necessary to aid in exploring the vast compositional landscape of multicomponent alloys. In an earlier study by Zepon et al., a thermodynamic model was introduced for calculating pressure-composition-temperature (PCT) diagrams of BCC multicomponent alloys [181]. To apply the model for alloy design, they further developed an open-source code, which was used to investigate the impact of various alloy metals (M) on the room temperatrure PCT diagrams of $Ti_{0.3}V_{0.3}Nb_{0.3}M_{0.1}$ alloys [182]. The $Ti_{0.3}V_{0.3}Nb_{0.3}Sc_{0.1}$ alloy showed an equilibrium plateau pressure that is three orders of magnitude lower than the base alloy. These findings demonstrate that the model and code can be effectively utilized to rapidly screen and predict a large number of alloys, serving as a valuable tool for alloy design. Fig. 12a and b shows the absorption-desorption curves of LaNiFeVMn before and after activation; it becomes clear that after activation, the absorption was very fast when compared to the inactivated product. Multiphase alloys with a mixture of BCC solid-solution and intermetallic Laves phase, have been found to have high hydrogen storage capacity and fast kinetics [183].
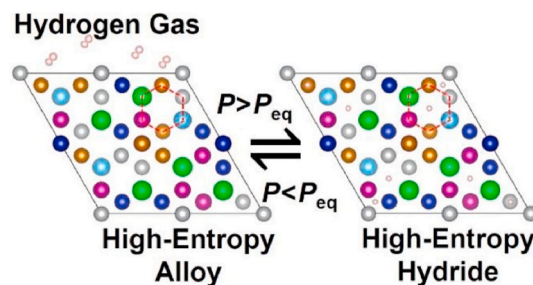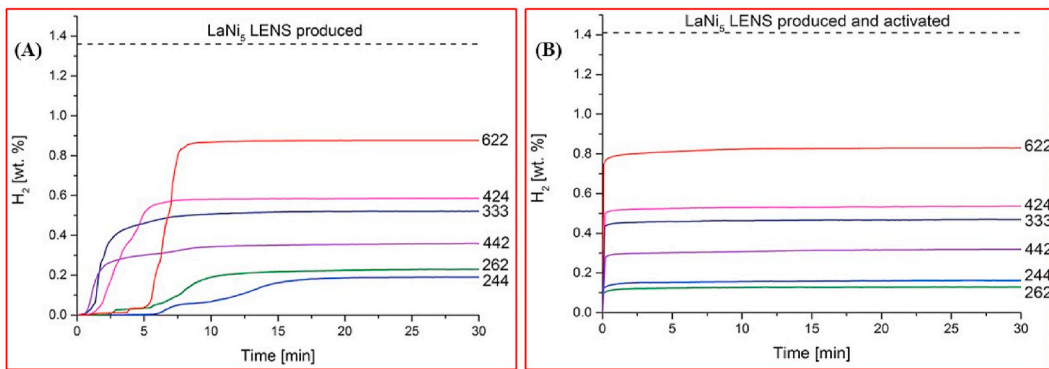

Fig. 11. Depiction of hydrogen uptake and release in high-entropy alloys and their respective hydrides. Reproduced from Ref. [170].

Fig. 12. Pressure-composition temperature absorption and desorption curves of LaNiFeVMn at 35 °C, **(a)** before activation & **(b)** after activation. Reproduced from Ref. [152].

For practical applications, desorption of hydrogen should occur under near-ambient conditions, i.e., temperature and pressure range of between 1 and 100 °C and between 1 and 10 atm, respectively [58,152,184]. Kao et al. [124], reported on the hydrogen storage properties of $CoFeMnTi_xV_yZr_z$ with a single C14 Laves phase structure. They found that the $CoFeMnTi_2VZr$ alloy exhibited maximum hydrogen capacity up to 1.8 wt% at room temperature. By varying the atomic percentage of $A\ell$ in the $A\ell_xCoCrFeNi$, three completely different microstructures with direct metal deposition techniques were obtained [54,120,185,186]. With the increase of the $A\ell$ content, the microstructure changed from the initial FCC to FCC/BCC and then completely, to the BCC phase [54,187]. Borkar et al. [53], carried out a systematic study of the role of Co and Cr in $A\ell Co_xCr_{1-x}FeNi$. The results highlighted the fact that the $A\ell CoFeNi$ ($x = 1$), have equiaxed B2 grains, hence, presenting an early stage of phase separation into Ni-$A\ell$-enriched and Fe–Co-enriched zones within the B2 phase, while for $x = 0$, the $A\ell CrFeNi$ exhibited grains with pronounced spinodal decomposition, leading to a BCC + B2 microstructure. Specifically, when $A\ell_xCoCrFeNi$ $x = 0.15–0.37$ the FCC phase was promoted, followed by a BCC/B2 precipitation in the FCC at $x = 0.41$. A further increase in $A\ell$ resulted in a BCC/B2 domination at $x = 0.69$ with the initiation of an FCC precipitation at the grain boundaries [25,54,120,126,185–189]. Kunce et al. investigated the hydrogen storage properties of ZrTiVCrFeNi manufactured by the LMD process and the absorption-desorption curves are shown in Fig. 13a [2].

After the material was synthesized, it was then annealed at 1000 °C for 24 h to improve the chemical composition. The alloy exhibited, mostly, a C14 Laves phase and a minor α-Ti solid solution, following a direct laser synthesis and additional annealing procedures. The measurements for H_2 storage capacity were conducted at a pressure of up to 100 bar and a temperature of 50 °C, and the sample was activated at 500 °C for 2 h. As shown in Fig. 13a, it was observed that maximum H_2 capacity of 1.81 wt% after synthesis and 1.56 wt% after annealing were achievable. However, the equilibrium pressure of hydrogen desorption was too low for a complete desorption. An interesting analysis is a comparison with a TiZrVCrFeNi, synthesized by a vacuum arc melting process that can undergo reversible hydrogen storage at room temperature without any activation, see Fig. 13b [180]. This material had a H_2 capacity of 1.6 wt % from the first cycle, and a H_2 capacity of 1.7 wt% on the third cycle. Moreover, the material desorbed hydrogen completely with almost no hysteresis in the pressure-composition temperature isotherms, as shown in Fig. 13b.

$A\ell_xCoCrFeNi$ and $A\ell_xCuFeNiCoCr$ HEAs, not only have excellent microstructural, corrosion, and mechanical properties, but strong single-phases of FCC and BCC were observed, which are desirable for H_2 storage applications [12,15,17–20,120]. Detailed investigations of $A\ell CoCrCuFeNi$ by the transmission electron microscope, showed that the alloy contained a distorted ordered BCC phase with a domain-like structure of a few nanometers in size, and its decomposition was governed by the enthalpies of mixing of the binary systems [17,36,190]. A refractory HEA, HfNbTiVZr, was fabricated by vacuum arc melting, and the hydrogenation measurements were carried out at an elevated temperatures of 289 °C, 317 °C, and 341 °C [191]. The maximum capacity observed was 1.9 H/M at 10 bars, irrespective of the temperature used for the evaluation.

6. Conclusion

Many computational programs and codes are now made open source in order to advance the prediction of selective phases and microstructural evolution analysis. The sole simple phases BCC, FCC, and their mixtures, need to simultaneously satisfy the following empirical conditions: $-22 \leq \Delta H_{mix} \leq 7 \text{ kJ mol}^{-1}$, $\Delta\delta \leq 8.5$, and $11 \leq \Delta S_{mix} \leq 19.5 \text{ JK}^{-1}\text{mol}^{-1}$ to be formed. FCC phases are found to be stable at higher $VEC \geq 8$, and BCC phases are stable at low $VEC < 6.87$. As analyzed above, the value of Ω is positive, and when $\Omega = 1$ should be proposed as a critical value to form the solid solution. If $\Omega > 1$, the contribution of $T\Delta S_{mix}$ will exceed that of ΔH_{mix} for a solid-solution formation, and the multi-component HEAs are mainly composed of the solid solutions; if $\Omega \leq 1$, ΔH_{mix} is the predominant part of the free energy, and intermetallic compounds and segregations before solid-solution phases to form in multi-component HEAs. The core HEA effects collectively define the unique behavior and performance of HEAs, making them promising candidates for advanced engineering applications. Laser metal deposition (LMD) is the most commonly employed technique for fabricating refractory high entropy alloys, surpassing other methods in usage, thus making it particularly suitable for H_2 storage. Proper tuning of P_{eq} in HEA hydrides ensures efficient hydrogen absorption and desorption at practical temperatures and pressures, making them ideal for storage
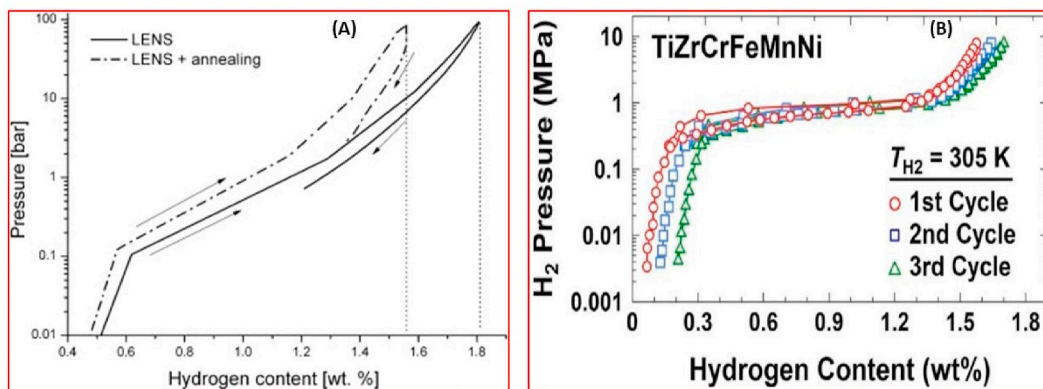
Fig. 13. (a) Pressure-composition temperature absorption and desorption curves of ZrTiVCrFeNi at 50 °C. Reproduced from Ref. [2]. **(b)** Pressure-composition temperature absorption and desorption curves of TiZrCrMnFeNi at 32 °C. Reproduced from Ref. [180].

applications. By addressing the seamless homogeneity of phases thereby increasing H_2 absorption. HEAs manufactured via AM can emerge as efficient, durable, and environmentally sustainable solutions for hydrogen storage, contributing to the transition towards a cleaner energy future. Collaborative efforts between researchers specializing in hydrogen storage technologies are crucial for advancing HEAs as viable alternative means for hydrogen storage applications.

Data availability statement

This manuscript is a review paper and does not contain any numerical or experimental data to disclose.

CRediT authorship contribution statement

Morena S. Xaba: Writing – review & editing, Writing – original draft, Conceptualization.

Declaration of competing interest

The authors declare that they have no known competing financial interests or personal relationships that could have appeared to influence the work reported in this paper.

Acknowledgments

References

[1] B. Cantor, Multicomponent high-entropy Cantor alloys, Prog. Mater. Sci. 120 (2021) 100754.
[2] I. Kunce, M. Polanski, J. Bystrzycki, Structure and hydrogen storage properties of a high entropy ZrTiVCrFeNi alloy synthesized using Laser Engineered Net Shaping (LENS), Int. J. Hydrogen Energy 38 (2013) 12180–12189.
[3] J.W. Yeh, S.K. Chen, S.J. Lin, J.Y. Gan, T.S. Chin, T.T. Shun, C.H. Tsau, S.Y. Chang, Nanostructured high-entropy alloys with multiple principal elements: novel alloy design concepts and outcomes, Adv. Eng. Mater. 6 (2004) 299–303.
[4] B. Cantor, I.T.H. Chang, P. Knight, A.J.B. Vincent, Microstructural development in equiatomic multicomponent alloys, Mater. Sci. Eng. A. 375–377 (2004) 213–218.
[5] F. Yang, J. Wang, Y. Zhang, Z. Wu, Z. Zhang, F. Zhao, J. Huot, J. Grobivć Novaković, N. Novaković, Recent progress on the development of high entropy alloys (HEAs) for solid hydrogen storage: a review, Int. J. Hydrogen Energy 47 (2022) 11236–11249.
[6] D.B. Miracle, High entropy alloys as a bold step forward in alloy development, Nat. Commun. 10 (2019) 1805.
[7] E.P. George, D. Raabe, R.O. Ritchie, High-entropy alloys, Nat. Rev. Mater. 4 (2019) 515–534.
[8] S. Gorsse, J. Couzinié, D.B. Miracle, Comptes Rendus Physique from high-entropy alloys to complex concentrated alloys, Compt. Rendus Phys. 19 (2018) 721–736.
[9] J.W. Yeh, Recent progress in high-entropy alloys, Ann. Chim. Sci. Des Mater 31 (2006) 633–648.
[10] A.D. Akinwekomi, F. Akhtar, Bibliometric Mapping of literature on high-entropy/multicomponent alloys and systematic review of emerging applications, Entropy 24 (2022) 329.
[11] J.L. Cann, A. De Luca, D.C. Dunand, D. Dye, D.B. Miracle, H.S. Oh, E.A. Olivetti, T.M. Pollock, W.J. Poole, R. Yang, C.C. Tasan, Sustainability through alloy design: challenges and opportunities, Prog. Mater. Sci. 117 (2021) 100722.
[12] W. Zhang, A. Chabok, B.J. Kooi, Y. Pei, Additive manufactured high entropy alloys: a review of the microstructure and properties, Mater. Des. 220 (2022) 110875.
[13] S. Sohn, Y. Liu, J. Liu, P. Gong, S. Prades-Rodel, A. Blatter, B.E. Scanley, C.C. Broadbridge, J. Schroers, Noble metal high entropy alloys, Scripta Mater. 126 (2017) 29–32.
[14] M. Dada, P. Popoola, O. Aramide, N. Mathe, S. Pityana, Optimization of the corrosion property of a high entropy alloy using response surface methodology, Mater. Today Proc. 38 (2021) 1024–1030.

[15] M. Dada, P. Popoola, N. Mathe, S. Pityana, S. Adeosun, O. Aramide, The comparative study of the microstructural and corrosion behaviour of laser-deposited high entropy alloys, J. Alloys Compd. 866 (2021) 158777.

[16] W. Cui, W. Li, W.T. Chen, F. Liou, Laser metal deposition of an AlCoCrFeNiTi0.5 high-entropy alloy coating on a Ti6Al4V substrate: microstructure and oxidation behavior, Crystals 10 (2020) 638.

[17] Y. Wang, R. Li, P. Niu, Z. Zhang, T. Yuan, J. Yuan, K. Li, Microstructures and properties of equimolar AlCoCrCuFeNi high-entropy alloy additively manufactured by selective laser melting, Intermetallics 120 (2020) 106746.

[18] Y. Fu, C. Dai, H. Luo, D. Li, C. Du, X. Li, The corrosion behavior and film properties of Al-containing high-entropy alloys in acidic solutions, Appl. Surf. Sci. 560 (2021) 149854.

[19] Y. Garip, N. Ergin, O. Ozdemir, Resistance sintering of CoCrFeNiAlx (x = 0.7, 0.85, 1) high entropy alloys: microstructural characterization, oxidation and corrosion properties, J. Alloys Compd. 877 (2021) 160180.

[20] R. Hu, J Du, Y. Zhang, Q. Ji, R. Zhang, J. Chen, Microstructure and corrosion properties of AlxCuFeNiCoCr (x = 0.5, 1.0, 1.5, 2.0) high entropy alloys with Al content, J. Alloys Compd. 921 (2022) 165455.

[21] H. Kumar, G.A. Bhaduri, S.G.K. Manikandan, M. Kamaraj, S. Shiva, Influence of annealing on microstructure and tribological properties of AlCoCrFeNiTi high entropy alloy based coating, Met. Mater. Int. 29 (2023) 645–658.

[22] E.W. Huang, D. Yu, J.W. Yeh, C. Lee, K. An, S.Y. Tu, A study of lattice elasticity from low entropy metals to medium and high entropy alloys, Scripta Mater. 101 (2015) 32–35.

[23] S. Liu, D. Wan, S. Guan, Y. Fu, X. Ren, Z. Zhang, J. He, Microstructure and nanomechanical behavior of an additively manufactured (CrCoNiFe)94Ti2Al4 high-entropy alloy, Mater. Sci. Eng. A. 823 (2021) 141737.

[24] Y.J. Zhou, Y. Zhang, Y.L. Wang, G.L. Chen, Solid solution alloys of AlCoCrFeNi Tix with excellent room-temperature mechanical properties, Appl. Phys. Lett. 90 (2007) 181904.

[25] H.R. Sistla, J.W. Newkirk, F. Frank Liou, Effect of Al/Ni ratio, heat treatment on phase transformations and microstructure of AlxFeCoCrNi2-x (x=0.3, 1) high entropy alloys, Mater. Des. 81 (2015) 113–121.

[26] D. Modupeola, P. Popoola, High entropy nanomaterials for energy storage and catalysis applications, Front. Energy Res. 11 (2023) 1149446.

[27] Z.U. Arif, M.Y. Khalid, A. Al Rashid, E. ur Rehman, M. Atif, Laser deposition of high-entropy alloys: a comprehensive review, Opt. Laser Technol. 145 (2022) 107447.

[28] X. Wang, W. Guo, Y. Fu, High-entropy alloys: emerging materials for advanced functional applications, J. Mater. Chem. A. 9 (2021) 663–701.

[29] W. Steurer, Single-phase high-entropy alloys – a critical update, Mater. Char. 162 (2020) 110179.

[30] J. Kim, A. Wakai, A. Moridi, Materials and manufacturing renaissance: additive manufacturing of high-entropy alloys, J. Mater. Res. 35 (2020) 1963–1983.

[31] S. Guo, C. Ng, J. Lu, C.T. Liu, Effect of valence electron concentration on stability of fcc or bcc phase in high entropy alloys, J. Appl. Phys. 109 (2011) 103505.

[32] C.-J. Tong, Y.-L. Chen, S.-K. Chen, J.-W. Yeh, T.-T. Shun, C.-H. Tsau, S.-J. Lin, S.-Y. Chang, Microstructure characterization of Al x CoCrCuFeNi high-entropy alloy system with multiprincipal elements, Metall. Mater. Trans. A. 36A (2005) 881.

[33] Y. Zhang, History of high-entropy materials, in: High-Entropy Mater. A Br. Introd., Springer Singapore, Singapore, 2019, pp. 1–33.

[34] R. Li, L. Xie, W.Y. Wang, P.K. Liaw, Y. Zhang, High-throughput calculations for high-entropy alloys: a brief review, Front. Mater. 7 (2020) 290.

[35] W. Al Zoubi, R.A.K. Putri, M.R. Abukhadra, Y.G. Ko, Recent experimental and theoretical advances in the design and science of high-entropy alloy nanoparticles, Nano Energy 110 (2023) 108362.

[36] B.A. Welk, R.E.A. Williams, G.B. Viswanathan, M.A. Gibson, P.K. Liaw, H.L. Fraser, Nature of the interfaces between the constituent phases in the high entropy alloy CoCrCuFeNiAl, Ultramicroscopy 134 (2013) 193–199.

[37] A. Amiri, R. Shahbazian-Yassar, Recent progress of high-entropy materials for energy storage and conversion, J. Mater. Chem. A. 9 (2021) 782–823.

[38] Z. Tang, S. Zhang, R. Cai, Q. Zhou, H. Wang, Designing high entropy alloys with dual fcc and bcc solid-solution phases: structures and mechanical properties, Metall. Mater. Trans. A Phys. Metall. Mater. Sci. 50 (2019) 1888–1901.

[39] M.C. Troparevsky, J.R. Morris, P.R.C. Kent, A.R. Lupini, G.M. Stocks, Criteria for predicting the formation of single-phase high-entropy alloys, Phys. Rev. X 5 (2015) 011041.

[40] C. Chattopadhyay, A. Prasad, B.S. Murty, Phase prediction in high entropy alloys – a kinetic approach, Acta Mater. 153 (2018) 214–225.

[41] O.B. Melnick, V.K. Soolshenko, K.H. Levchuk, Thermodynamic prediction of phase composition of transition metals high-entropy alloys, Met. Adv. Technol. 42 (2020) 1387–1400.

[42] L. Hatzenbichler, S. Zeisl, H. Clemens, D. Holec, Phase stability of TiAl-based BCC high entropy alloys, Intermetallics 158 (2023) 107893.

[43] S. Guo, Phase selection rules for cast high entropy alloys: an overview, Mater. Sci. Technol. 31 (2015) 1223–1230.

[44] R. Feng, P.K. Liaw, M.C. Gao, M. Widom, First-principles prediction of high-entropy-alloy stability, npj Comput. Mater. 3 (2017) 50.

[45] O.N. Senkov, J.D. Miller, D.B. Miracle, C. Woodward, Accelerated exploration of multi-principal element alloys for structural applications, Calphad Comput. Coupling Phase Diagrams Thermochem. 50 (2015) 32–48.

[46] D. Miracle, B. Majumdar, K. Wertz, S. Gorsse, New strategies and tests to accelerate discovery and development of multi-principal element structural alloys, Scripta Mater. 127 (2017) 195–200.

[47] K. Kong, J. Hyun, Y. Kim, W. Kim, D. Kim, Nanoporous structure synthesized by selective phase dissolution of AlCoCrFeNi high entropy alloy and its electrochemical properties as supercapacitor electrode, J. Power Sources 437 (2019) 226927.

[48] X.F. Wang, Y. Zhang, Y. Qiao, G.L. Chen, Novel microstructure and properties of multicomponent CoCrCuFeNiTix alloys, Intermetallics 15 (2007) 357–362.

[49] Y. Zhang, T.T. Zuo, Z. Tang, M.C. Gao, K.A. Dahmen, P.K. Liaw, Z.P. Lu, Microstructures and properties of high-entropy alloys, Prog. Mater. Sci. 61 (2014) 1–93.

[50] C. Zhang, J. Zhu, H. Zheng, H. Li, S. Liu, G.J. Cheng, A review on microstructures and properties of high entropy alloys manufactured by selective laser melting, Int. J. Extrem. Manuf. 2 (2020) 032003.

[51] K. Sun, W. Peng, L. Yang, L. Fang, Effect of SLM processing parameters on microstructures and mechanical properties of Al0, 5CoCrFeNi high entropy alloys, Metals (Basel) 10 (2020) 292.

[52] I. Kunce, M. Polanski, J. Bystrzycki, Microstructure and hydrogen storage properties of a TiZrNbMoV high entropy alloy synthesized using Laser Engineered Net Shaping (LENS), Int. J. Hydrogen Energy 39 (2014) 9904–9910.

[53] T. Borkar, V. Chaudhary, B. Gwalani, D. Choudhuri, C.V. Mikler, V. Soni, T. Alam, R.V. Ramanujan, R. Banerjee, A combinatorial approach for assessing the magnetic properties of high entropy alloys: role of Cr in AlCoxCr1–xFeNi, Adv. Eng. Mater. 19 (2017) 1700048.

[54] T. Borkar, B. Gwalani, D. Choudhuri, C.V. Mikler, C.J. Yannetta, X. Chen, R.V. Ramanujan, M.J. Styles, M.A. Gibson, R. Banerjee, A combinatorial assessment of AlxCrCuFeNi2 (0 < x < 1.5) complex concentrated alloys: microstructure, microhardness, and magnetic properties, Acta Mater. 116 (2016) 63–76.

[55] Y. Mizuguchi, Superconductivity in high-entropy-alloy telluride AgInSnPbBiTe5, J. Phys. Soc. Japan 88 (2019) 124708.

[56] S.-G. Jung, Y. Han, J.H. Kim, R. Hidayati, J.-S. Rhyee, J.M. Lee, W.N. Kang, W.S. Choi, H.-R. Jeon, J. Suk, T. Park, High critical current density and high-tolerance superconductivity in high-entropy alloy thin films, Nat. Commun. 13 (2022) 3373.

[57] K. Stolze, J. Tao, F.O. von Rohr, T. Kong, R.J. Cava, Sc–Zr–Nb–Rh–Pd and Sc–Zr–Nb–Ta–Rh–Pd high-entropy alloy superconductors on a CsCl-type lattice, Chem. Mater. 30 (2018) 906–914.

[58] L. Kong, B. Cheng, D. Wan, Y. Xue, A review on BCC-structured high-entropy alloys for hydrogen storage, Front. Mater. 10 (2023) 1135864.

[59] C. Zlotea, M.A. Sow, G. Ek, J.P. Couzinié, L. Perrière, I. Guillot, J. Bourgon, K.T. Møller, T.R. Jensen, E. Akiba, M. Sahlberg, Hydrogen sorption in TiZrNbHfTa high entropy alloy, J. Alloys Compd. 775 (2019) 667–674.

[60] B. Sarac, V. Zadorozhnyy, E. Berdonosova, Y.P. Ivanov, S. Klyamkin, S. Gumrukcu, A.S. Sarac, A. Korol, D. Semenov, M. Zadorozhnyy, A. Sharma, A.L. Greer, J. Eckert, Hydrogen storage performance of the multi-principal-component CoFeMnTiVZr alloy in electrochemical and gas-solid reactions, RSC Adv. 10 (2020) 24613–24623.

[61] K.A. Christofidou, T.P. McAuliffe, P.M. Mignanelli, H.J. Stone, N.G. Jones, On the prediction and the formation of the sigma phase in CrMnCoFeNix high entropy alloys, J. Alloys Compd. 770 (2019) 285–293.
[62] Y. Lederer, C. Toher, K.S. Vecchio, S. Curtarolo, The search for high entropy alloys: a high-throughput ab-initio approach, Acta Mater. 159 (2018) 364–383.
[63] L.J. Santodonato, P.K. Liaw, R.R. Unocic, H. Bei, J.R. Morris, Predictive multiphase evolution in Al-containing high-entropy alloys, Nat. Commun. 9 (2018) 4520.
[64] Z.S. Nong, J.C. Zhu, R. Da Zhao, Prediction of structure and elastic properties of AlCrFeNiTi system high entropy alloys, Intermetallics 86 (2017) 134–146.
[65] J. Li, K. Yamanaka, A. Chiba, Calculation-driven design of off-equiatomic high-entropy alloys with enhanced solid-solution strengthening, Mater. Sci. Eng. A. 817 (2021) 141359.
[66] R. Puerling, A. Miklas, F.G. Coury, N.R. Philips, P. Mason, N.E. Peterson, A. Deal, J. Klemm-Toole, A.J. Clarke, Thermodynamics and kinetics of refractory multi-principal element alloys: an experimental and modeling comparison, Metall. Mater. Trans. A Phys. Metall. Mater. Sci. 54A (2023) 1070.
[67] I. Toda-Caraballo, J.S. Wróbel, D. Nguyen-Manh, P. Pérez, P.E.J. Rivera-Díaz-del-Castillo, Simulation and modeling in high entropy alloys, J. Miner. Met. Mater. Soc. 69 (2017) 2137–2149.
[68] F. Otto, Y. Yang, H. Bei, E.P. George, Relative effects of enthalpy and entropy on the phase stability of equiatomic high-entropy alloys, Acta Mater. 61 (2013) 2628–2638.
[69] P. Martin, C.E. Madrid-Cortes, C. Cáceres, N. Araya, C. Aguilar, J.M. Cabrera, HEAPS: a user-friendly tool for the design and exploration of high-entropy alloys based on semi-empirical parameters, Comput. Phys. Commun. 278 (2022) 108398.
[70] C. Haase, F. Tang, M.B. Wilms, A. Weisheit, B. Hallstedt, Combining thermodynamic modeling and 3D printing of elemental powder blends for high-throughput investigation of high-entropy alloys – towards rapid alloy screening and design, Mater. Sci. Eng. A. 688 (2017) 180–189.
[71] M.C. Gao, D.E. Alman, Searching for next single-phase high-entropy alloy compositions, Entropy 15 (2013) 4504–4519.
[72] Tazuddin, N.P. Gurao, K. Biswas, In the quest of single phase multi-component multiprincipal high entropy alloys, J. Alloys Compd. 697 (2017) 434–442.
[73] B. Cheng, L. Kong, H. Cai, Y. Li, Y. Zhao, D. Wan, Y. Xue, Pushing the Boundaries of solid-state hydrogen storage: a Refined study on TiVNbCrMo high-entropy alloys, Int. J. Hydrogen Energy 60 (2024) 282–292.
[74] F. Zareipour, H. Shahmir, Y. Huang, Formation and significance of topologically close-packed Laves phases in refractory high-entropy alloys, J. Alloys Compd. 986 (2024) 174148.
[75] B. Dong, Z. Wang, H. Zhu, O. Muránsky, Z. Qiu, C. Shen, Z. Pan, H. Li, Low neutron cross-section FeCrVTiNi based high-entropy alloys: design, additive manufacturing and characterization, Microstructures 2 (2022) 2022003.
[76] M.D. Witman, S. Ling, M. Wadge, A. Bouzidi, N. Pineda-Romero, R. Clulow, G. Ek, J.M. Chames, E.J. Allendorf, S. Agarwal, M.D. Allendorf, G.S. Walker, D. M. Grant, M. Sahlberg, C. Zlotea, V. Stavila, Towards Pareto optimal high entropy hydrides via data-driven materials discovery, J. Mater. Chem. A. 11 (2023) 15878–15888.
[77] D.B. Miracle, O.N. Senkov, A critical review of high entropy alloys and related concepts, Acta Mater. 122 (2017) 448–511.
[78] B.S. Murty, J.W. Yeh, S. Ranganathan, P.P. Bhattacharjee, High-Entropy Alloys, second ed., Elsevier, 2014.
[79] Y. Zhang, Y.J. Zhou, J.P. Lin, G.L. Chen, P.K. Liaw, Solid-solution phase formation rules for multi-component alloys, Adv. Eng. Mater. 10 (2008) 534–538.
[80] X. Yang, Y. Zhang, Prediction of high-entropy stabilized solid-solution in multi-component alloys, Mater. Chem. Phys. 132 (2012) 233–238.
[81] S. Guo, Q. Hu, C. Ng, C.T. Liu, More than entropy in high-entropy alloys: forming solid solutions or amorphous phase, Intermetallics 41 (2013) 96–103.
[82] A. Takeuchi, K. Amiya, T. Wada, K. Yubuta, W. Zhang, A. Makino, Entropies in alloy design for high-entropy and bulk glassy alloys, Entropy 15 (2013) 3810–3821.
[83] Y. Zhang, X. Yang, P.K. Liaw, Alloy design and properties optimization of high-entropy alloys, JMET (J. Med. Eng. Technol.) 64 (2012) 830–838.
[84] Z.-S. Nong, J.-C. Zhu, Y. Cao, X.-W. Yang, Z.-H. Lai, Y. Liu, Stability and structure prediction of cubic phase in as cast high entropy alloys, Mater. Sci. Technol. 30 (2014) 363–369.
[85] O.N. Senkov, D.B. Miracle, A new thermodynamic parameter to predict formation of solid solution or intermetallic phases in high entropy alloys, J. Alloys Compd. 658 (2016) 603–607.
[86] Y.F. Ye, Q. Wang, J. Lu, C.T. Liu, Y. Yang, The generalized thermodynamic rule for phase selection in multicomponent alloys, Intermetallics 59 (2015) 75–80.
[87] M.G. Poletti, L. Battezzati, Electronic and thermodynamic criteria for the occurrence of high entropy alloys in metallic systems, Acta Mater. 75 (2014) 297–306.
[88] Z. Wang, Y. Huang, Y. Yang, J. Wang, C.T. Liu, Atomic-size effect and solid solubility of multicomponent alloys, Scripta Mater. 94 (2015) 28–31.
[89] A.B. Melnick, V.K. Soolshenko, Thermodynamic design of high-entropy refractory alloys, J. Alloys Compd. 694 (2017) 223–227.
[90] M.S.M.S. Xaba, R. Meijboom, Kinetic and catalytic analysis of mesoporous Co3O4 on the oxidation of morin, Appl. Surf. Sci. 423 (2017) 53–62.
[91] A. Takeuchi, A. Inoue, Quantitative evaluation of critical cooling rate for metallic glasses, A304, Mater. Sci. Eng 306 (2001) 446–451.
[92] G. Qin, Z. Li, R. Chen, H. Zheng, C. Fan, L. Wang, Y. Su, H. Ding, J. Guo, H. Fu, CoCrFeMnNi high-entropy alloys reinforced with Laves phase by adding Nb and Ti elements, J. Mater. Res. 34 (2019) 1011–1020.
[93] D.J.M. King, S.C. Middleburgh, A.G. McGregor, M.B. Cortie, Predicting the formation and stability of single phase high-entropy alloys, Acta Mater. 104 (2016) 172–179.
[94] S.A. Kube, J. Schroers, Metastability in high entropy alloys, Scripta Mater. 186 (2020) 392–400.
[95] J. Du, L. Liu, Y. Yu, Y. Qin, H. Wu, A. Chen, A confined space pyrolysis strategy for controlling the structure of hollow mesoporous carbon spheres with high supercapacitor performance, Nanoscale 11 (2019) 4453–4462.
[96] S. Guo, C.T. Liu, Phase stability in high entropy alloys: formation of solid-solution phase or amorphous phase, Prog. Nat. Sci. Mater. Int. 21 (2011) 433–446.
[97] M.X. Ren, B.S. Li, H.Z. Fu, Formation condition of solid solution type high-entropy alloy, Trans. Nonferrous Metals Soc. China 23 (2013) 991–995 (English Ed.
[98] Y.F. Ye, X.D. Liu, S. Wang, C.T. Liu, Y. Yang, The general effect of atomic size misfit on glass formation in conventional and high-entropy alloys, Intermetallics 78 (2016) 30–41.
[99] M.H. Tsai, J.W. Yeh, High-entropy alloys: a critical review, Mater. Res. Lett. 2 (2014) 107–123.
[100] S. Fang, X. Xiao, L. Xia, W. Li, Y. Dong, Relationship between the widths of supercooled liquid regions and bond parameters of Mg-based bulk metallic glasses, J. Non-Cryst. Solids 321 (2003) 120–125.
[101] A. Kumar, P. Dhekne, A.K. Swarnakar, M.K. Chopkar, Analysis of Si addition on phase formation in AlCoCrCuFeNiSix high entropy alloys, Mater. Lett. 188 (2017) 73–76.
[102] R. Chen, G. Qin, H. Zheng, L. Wang, Y. Su, Y.L. Chiu, H. Ding, J. Guo, H. Fu, Composition design of high entropy alloys using the valence electron concentration to balance strength and ductility, Acta Mater. 144 (2018) 129–137.
[103] W.-L. Hsu, C.-W. Tsai, A.-C. Yeh, J.-W. Yeh, Clarifying the four core effects of high-entropy materials, Nat. Rev. Chem. 8 (2024) 471–485.
[104] Y. Ma, Y. Ma, Q. Wang, S. Schweidler, M. Botros, T. Fu, H. Hahn, T. Brezesinski, B. Breitung, High-entropy energy materials: challenges and new opportunities, Energy Environ. Sci. 14 (2021) 2883–2905.
[105] M.F. Del Grosso, G. Bozzolo, H.O. Mosca, Determination of the transition to the high entropy regime for alloys of refractory elements, J. Alloys Compd. 534 (2012) 25–31.
[106] I. Toda-Caraballo, P.E.J. Rivera-Díaz-Del-Castillo, A criterion for the formation of high entropy alloys based on lattice distortion, Intermetallics 71 (2016) 76–87.
[107] M.H. Tsai, Physical properties of high entropy alloys, Entropy 15 (2013) 5338–5345.
[108] M.C. Gao, D.B. Miracle, D. Maurice, X. Yan, Y. Zhang, J.A. Hawk, High-entropy functional materials, J. Mater. Res. 33 (2018) 3138–3155.
[109] Y. Zou, S. Maiti, W. Steurer, R. Spolenak, Size-dependent plasticity in an Nb25Mo25Ta25W25 refractory high-entropy alloy, Acta Mater. 65 (2014) 85–97.
[110] S. Chen, L. Wang, L. Wang, Y. Xue, B. Wang, Enhanced phase stability of a BCC structure system high-entropy alloys by decreasing elastic distortion energy, in: J. Phys. Conf. Ser., IOP Publishing Ltd, 2021 012207.
[111] J. Dąbrowa, M. Danielewski, State-of-the-art diffusion studies in the high entropy alloys, Metals 10 (2020).

[112] K.Y. Tsai, M.H. Tsai, J.W. Yeh, Sluggish diffusion in Co-Cr-Fe-Mn-Ni high-entropy alloys, Acta Mater. 61 (2013) 4887–4897.

[113] S. Ranganathan, Alloyed pleasures: multimetallic cocktails, Curr. Sci. 85 (2003) 1404.

[114] P. Badoniya, M. Srivastava, P.K. Jain, S. Rathee, A state-of-the-art review on metal additive manufacturing: milestones, trends, challenges and perspectives, J. Brazilian Soc. Mech. Sci. Eng. 46 (2024) 339.

[115] E. Claus, J. Kranz, H. Dirk, W. Eric, Laser additive manufacturing of metals, in: Volker M.R. Schmidt, Belegratis (Eds.), Laser Technol. Biomimetics Basics Appl., Springer, Berlin Heidelberg, Berlin, Heidelberg, 2013, pp. 143–162.

[116] D. Herzog, V. Seyda, E. Wycisk, C. Emmelmann, Additive manufacturing of metals, Acta Mater. 117 (2016) 371–392.

[117] Y. Liu, Y. Ding, L. Yang, R. Sun, T. Zhang, X. Yang, Research and progress of laser cladding on engineering alloys: a review, J. Manuf. Process. 66 (2021) 341–363.

[118] T.H. Becker, P. Kumar, U. Ramamurty, Fracture and fatigue in additively manufactured metals, Acta Mater. 219 (2021).

[119] N. Li, S. Huang, G. Zhang, R. Qin, W. Liu, H. Xiong, G. Shi, J. Blackburn, Progress in additive manufacturing on new materials: a review, J. Mater. Sci. Technol. 35 (2019) 242–269.

[120] J. Joseph, T. Jarvis, X. Wu, N. Stanford, P. Hodgson, D.M. Fabijanic, Comparative study of the microstructures and mechanical properties of direct laser fabricated and arc-melted AlxCoCrFeNi high entropy alloys, Mater. Sci. Eng. A 633 (2015) 184–193.

[121] X. Li, Additive manufacturing of advanced multi-component alloys: bulk metallic glasses and high entropy alloys, Adv. Eng. Mater. 20 (2018) 1700874.

[122] C.M. Lin, H.L. Tsai, Evolution of microstructure, hardness, and corrosion properties of high-entropy Al0.5CoCrFeNi alloy, Intermetallics 19 (2011) 288–294.

[123] C. Zhang, A. Song, Y. Yuan, Y. Wu, P. Zhang, Z. Lu, X. Song, Study on the hydrogen storage properties of a TiZrNbTa high entropy alloy, Int. J. Hydrogen Energy 45 (2020) 5367–5374.

[124] Y.F. Kao, S.K. Chen, J.H. Sheu, J.T. Lin, W.E. Lin, J.W. Yeh, S.J. Lin, T.H. Liou, C.W. Wang, Hydrogen storage properties of multi-principal-component CoFeMnTi xVyZrz alloys, Int. J. Hydrogen Energy 35 (2010) 9046–9059.

[125] P.E.J. Rivera-Díaz-Del-Castillo, H. Fu, Strengthening mechanisms in high-entropy alloys: perspectives for alloy design, J. Mater. Res. 33 (2018) 2970–2982.

[126] I. Kunce, M. Polanski, K. Karczewski, T. Plocinski, K.J. Kurzydlowski, Microstructural characterisation of high-entropy alloy AlCoCrFeNi fabricated by laser engineered net shaping, J. Alloys Compd. 648 (2015) 751–758.

[127] H. Dobbelstein, E.L. Gurevich, E.P. George, A. Ostendorf, G. Laplanche, Laser metal deposition of compositionally graded TiZrNbTa refractory high-entropy alloys using elemental powder blends, Addit. Manuf. 25 (2019) 252–262.

[128] H. Dobbelstein, M. Thiele, E.L. Gurevich, E.P. George, A. Ostendorf, Direct metal deposition of refractory high entropy alloy MoNbTaW, in: Phys. Procedia, Elsevier B.V., 2016, pp. 624–633.

[129] I. Maskery, N.T. Aboulkhair, M.R. Corfield, C. Tuck, A.T. Clare, R.K. Leach, R.D. Wildman, I.A. Ashcroft, R.J.M. Hague, Quantification and characterisation of porosity in selectively laser melted Al-Si10-Mg using X-ray computed tomography, Mater. Char. 111 (2016) 193–204.

[130] W.E. Frazier, Metal additive manufacturing: a review, J. Mater. Eng. Perform. 23 (2014) 1917–1928.

[131] L. Löber, F.P. Schimansky, U. Kühn, F. Pyczak, J. Eckert, Selective laser melting of a beta-solidifying TNM-B1 titanium aluminide alloy, J. Mater. Process. Technol. 214 (2014) 1852–1860.

[132] L.E. Murr, S.M. Gaytan, A. Ceylan, E. Martinez, J.L. Martinez, D.H. Hernandez, B.I. Machado, D.A. Ramirez, F. Medina, S. Collins, R.B. Wicker, Characterization of titanium aluminide alloy components fabricated by additive manufacturing using electron beam melting, Acta Mater. 58 (2010) 1887–1894.

[133] B. Van der Schueren, J.P. Kruth, Powder deposition in selective metal powder sintering, Rapid Prototyp. J. 1 (1995) 23–31.

[134] X. Gong, T. Anderson, K. Chou, Review on powder-based electron beam additive manufacturing Technology, Manuf. Rev. 1 (2014) 2.

[135] H.Y. Jung, N.J. Peter, E. Gärtner, G. Dehm, V. Uhlenwinkel, E.A. Jägle, Bulk nanostructured AlCoCrFeMnNi chemically complex alloy synthesized by laser-powder bed fusion, Addit. Manuf. 35 (2020) 101337.

[136] D. Lin, L. Xu, H. Jing, Y. Han, L. Zhao, F. Minami, Effects of annealing on the structure and mechanical properties of FeCoCrNi high-entropy alloy fabricated via selective laser melting, Addit. Manuf. 32 (2020) 101058.

[137] F. Peyrouzet, D. Hachet, R. Soulas, C. Navone, S. Godet, S. Gorsse, Selective laser melting of Al0.3CoCrFeNi high-entropy alloy: printability, microstructure, and mechanical properties, JOM 71 (2019) 3443–3451.

[138] S. Chen, H.S. Oh, B. Gludovatz, S.J. Kim, E.S. Park, Z. Zhang, R.O. Ritchie, Q. Yu, Real-time observations of TRIP-induced ultrahigh strain hardening in a dual-phase CrMnFeCoNi high-entropy alloy, Nat. Commun. 11 (2020) 826.

[139] P. Chen, C. Yang, S. Li, M.M. Attallah, M. Yan, In-situ alloyed, oxide-dispersion-strengthened CoCrFeMnNi high entropy alloy fabricated via laser powder bed fusion, Mater. Des. 194 (2020) 108966.

[140] Y. Su, S. Luo, Z. Wang, Microstructure evolution and cracking behaviors of additively manufactured AlxCrCuFeNi2 high entropy alloys via selective laser melting, J. Alloys Compd. 842 (2020) 155823.

[141] A. Ozalp, C. Okuyucu, B. Koc, O. El-Atwani, E. Aydogan, Development and directed energy deposition of high strength Hf5Mo15Nb35Ta25Ti20 refractory high entropy alloys, Mater. Char. 209 (2024) 113679.

[142] P. Sreeramagiri, G. Balasubramanian, Directed energy deposition of multi-principal element alloys, Front. Mater. 9 (2022) 825276.

[143] S. Chen, Y. Tong, P.K. Liaw, Additive manufacturing of high-entropy alloys: a review, Entropy 20 (2018) 937.

[144] A. Ostovari Moghaddam, N.A. Shaburova, M.N. Samodurova, A. Abdollahzadeh, E.A. Trofimov, Additive manufacturing of high entropy alloys: a practical review, J. Mater. Sci. Technol. 77 (2021) 131–162.

[145] M.A. Melia, S.R. Whetten, R. Puckett, M. Jones, M.J. Heiden, N. Argibay, A.B. Kustas, High-throughput additive manufacturing and characterization of refractory high entropy alloys, Appl. Mater. Today 19 (2020) 100560.

[146] S. Guan, K. Solberg, D. Wan, F. Berto, T. Welo, T.M. Yue, K.C. Chan, Formation of fully equiaxed grain microstructure in additively manufactured AlCoCrFeNiTi0.5 high entropy alloy, Mater. Des. 184 (2019) 108202.

[147] Y.J. Zhou, Y. Zhang, T.N. Kim, G.L. Chen, Microstructure characterizations and strengthening mechanism of multi-principal component AlCoCrFeNiTi0.5 solid solution alloy with excellent mechanical properties, Mater. Lett. 62 (2008) 2673–2676.

[148] M. Dada, P. Popoola, N. Mathe, S. Pityana, S. Adeosun, Effect of laser parameters on the properties of high entropy alloys: a preliminary study, in: Mater. Today Proc., Elsevier Ltd, 2021, pp. 756–761.

[149] M. Dada, P. Popoola, N. Mathe, S. Pityana, S. Adeosun, O. Aramide, T. Lengopeng, Process optimization of high entropy alloys by laser additive manufacturing, Eng. Reports. 2 (2020) 12252.

[150] F. He, Z. Wang, P. Cheng, Q. Wang, J. Li, Y. Dang, J. Wang, C.T. Liu, Designing eutectic high entropy alloys of CoCrFeNiNbx, J. Alloys Compd. 656 (2016) 284–289.

[151] S. Guan, J. Ren, S. Mooraj, Y. Liu, S. Feng, S. Zhang, J. Liu, X. Fan, P.K. Liaw, W. Chen, Additive manufacturing of high-entropy alloys: microstructural metastability and mechanical behavior, J. Phase Equilibria Diffus. 42 (2021) 748–771.

[152] I. Kunce, M. Polański, T. Czujko, Microstructures and hydrogen storage properties of La–Ni–Fe–V–Mn alloys, Int. J. Hydrogen Energy 42 (2017) 27154–27164.

[153] H. Shen, J. Zhang, J. Hu, J. Zhang, Y. Mao, H. Xiao, X. Zhou, X. Zu, A novel TiZrHfMoNb high-entropy alloy for solar thermal energy storage, Nanomaterials 9 (2019) 248.

[154] T. Fujieda, H. Shiratori, K. Kuwabara, T. Kato, K. Yamanaka, Y. Koizumi, A. Chiba, First demonstration of promising selective electron beam melting method for utilizing high-entropy alloys as engineering materials, Mater. Lett. 159 (2015) 12–15.

[155] H. Shiratori, T. Fujieda, K. Yamanaka, Y. Koizumi, K. Kuwabara, T. Kato, A. Chiba, Relationship between the microstructure and mechanical properties of an equiatomic AlCoCrFeNi high-entropy alloy fabricated by selective electron beam melting, Mater. Sci. Eng. A 656 (2016) 39–46.

[156] K. Kuwabara, H. Shiratori, T. Fujieda, K. Yamanaka, Y. Koizumi, A. Chiba, Mechanical and corrosion properties of AlCoCrFeNi high-entropy alloy fabricated with selective electron beam melting, Addit. Manuf. 23 (2018) 264–271.

[157] K. Yamanaka, H. Shiratori, M. Mori, K. Omura, T. Fujieda, K. Kuwabara, A. Chiba, Corrosion mechanism of an equimolar AlCoCrFeNi high-entropy alloy additively manufactured by electron beam melting, npj Mater. Degrad. 4 (2020) 24.

[158] T. Fujieda, H. Shiratori, K. Kuwabara, M. Hirota, T. Kato, K. Yamanaka, Y. Koizumi, A. Chiba, S. Watanabe, CoCrFeNiTi-based high-entropy alloy with superior tensile strength and corrosion resistance achieved by a combination of additive manufacturing using selective electron beam melting and solution treatment, Mater. Lett. 189 (2017) 148–151.

[159] V. V Popov, A. Katz-Demyanetz, A. Koptyug, M. Bamberger, Selective electron beam melting of Al0.5CrMoNbTa0.5 high entropy alloys using elemental powder blend, Heliyon 5 (2019) e01188.

[160] M. Zhang, X. Zhou, D. Wang, L. He, X. Ye, W. Zhang, Additive manufacturing of in-situ strengthened dual-phase AlCoCuFeNi high-entropy alloy by selective electron beam melting, J. Alloys Compd. 893 (2022) 162259.

[161] B. Xiao, W. Jia, H. Tang, J. Wang, L. Zhou, Microstructure and mechanical properties of WMoTaNbTi refractory high-entropy alloys fabricated by selective electron beam melting, J. Mater. Sci. Technol. 108 (2022) 54–63.

[162] A. Takeuchi, A. Inoue, Classification of bulk metallic glasses by atomic size difference, heat of mixing and period of constituent elements and its application to characterization of the main alloying element, Mater. Trans. 46 (2005) 2817–2829.

[163] B. Xiao, H. Liu, W. Jia, J. Wang, L. Zhou, Cracking suppression in selective electron beam melted WMoTaNbC refractory high-entropy alloy, J. Alloys Compd. 948 (2023) 169787.

[164] B. Xiao, W. Jia, J. Wang, L. Zhou, Selective electron beam melting of WMoTaNbVFeCoCrNi refractory high-entropy alloy, Mater. Char. 193 (2022) 112278.

[165] N. Thakkar, P. Paliwal, Hydrogen storage based micro-grid: a comprehensive review on technology, energy management and planning techniques, Int. J. Green Energy 20 (2023) 445–463.

[166] Z. Free, M. Hernandez, M. Mashal, K. Mondal, A review on advanced manufacturing for hydrogen storage applications, Energies 14 (2021).

[167] K.L. Lim, H. Kazemian, Z. Yaakob, W.R.W. Daud, Solid-state materials and methods for hydrogen storage: a critical review, Chem. Eng. Technol. 33 (2010) 213–226.

[168] M. Bououdina, D. Grant, G. Walker, Review on hydrogen absorbing materials—structure, microstructure, and thermodynamic properties, Int. J. Hydrogen Energy 31 (2006) 177–182.

[169] A. Züttel, Materials for hydrogen storage, Mater. Today 6 (2003) 24–33.

[170] S. Dangwal, K. Edalati, High-entropy alloy TiV2ZrCrMnFeNi for hydrogen storage at room temperature with full reversibility and good activation, Scripta Mater. 238 (2024) 115774.

[171] B. Cheng, Y. Li, X. Li, H. Ke, L. Wang, T. Cao, D. Wan, B. Wang, Solid - state hydrogen storage properties of Ti – V – Nb – Cr high - entropy alloys and the associated effects of transitional metals (M = Mn , Fe , Ni), Acta Metall. Sin. English Lett. 36 (2023) 1113–1122.

[172] M.O. de Marco, Y. Li, H.W. Li, K. Edalati, R. Floriano, Mechanical synthesis and hydrogen storage characterization of MgVCr and MgVTiCrFe high-entropy alloy, Adv. Eng. Mater. 22 (2020).

[173] G. Zepon, D.R. Leiva, R.B. Strozi, A. Bedoch, S.J.A. Figueroa, T.T. Ishikawa, W.J. Botta, Hydrogen-induced phase transition of MgZrTiFe0.5Co0.5Ni0.5 high entropy alloy, Int. J. Hydrogen Energy 43 (2018) 1702–1708.

[174] R.B. Strozi, D.R. Leiva, J. Huot, W.J. Botta, G. Zepon, Synthesis and hydrogen storage behavior of Mg–V–Al–Cr–Ni high entropy alloys, Int. J. Hydrogen Energy 46 (2021) 2351–2361.

[175] M. Aoki, T. Noritake, A. Ito, M. Ishikiriyama, S.I. Towata, Improvement of cyclic durability of Ti-Cr-V alloy by Fe substitution, Int. J. Hydrogen Energy 36 (2011) 12329–12332.

[176] J. Huot, H. Enoki, E. Akiba, Synthesis, phase transformation, and hydrogen storage properties of ball-milled TiV0.9Mn1.1, J. Alloys Compd. 453 (2008) 203–209.

[177] M. Sahlberg, D. Karlsson, C. Zlotea, U. Jansson, Superior hydrogen storage in high entropy alloys, Sci. Rep. 6 (2016) 36770.

[178] S.K. Dewangan, V.K. Sharma, P. Sahu, V. Kumar, Synthesis and characterization of hydrogenated novel AlCrFeMnNiW high entropy alloy, Int. J. Hydrogen Energy 45 (2020) 16984–16991.

[179] S.K. Chen, P.H. Lee, H. Lee, H.T. Su, Hydrogen storage of C14-CruFevMnwTixVyZrz alloys, Mater. Chem. Phys. 210 (2018) 336–347.

[180] P. Edalati, R. Floriano, A. Mohammadi, Y. Li, G. Zepon, H.W. Li, K. Edalati, Reversible room temperature hydrogen storage in high-entropy alloy TiZrCrMnFeNi, Scripta Mater. 178 (2020) 387–390.

[181] G. Zepon, B.H. Silva, C. Zlotea, W.J. Botta, Y. Champion, Thermodynamic modelling of hydrogen-multicomponent alloy systems: calculating pressure-composition-temperature diagrams, Acta Mater. 215 (2021) 117070.

[182] O.A. Pedroso, W.J. Botta, G. Zepon, An open-source code to calculate pressure-composition-temperature diagrams of multicomponent alloys for hydrogen storage, Int. J. Hydrogen Energy 47 (2022) 32582–32593.

[183] E. Akiba, H. Iba, Hydrogen absorption by Laves phase related BCC solid solution, Intermetallics 6 (1998) 461–470.

[184] N.A.A. Rusman, M. Dahari, A review on the current progress of metal hydrides material for solid-state hydrogen storage applications, Int. J. Hydrogen Energy 41 (2016) 12108–12126.

[185] J. Joseph, N. Stanford, P. Hodgson, D.M. Fabijanic, Understanding the mechanical behaviour and the large strength/ductility differences between FCC and BCC AlxCoCrFeNi high entropy alloys, J. Alloys Compd. 726 (2017) 885–895.

[186] J. Joseph, P. Hodgson, T. Jarvis, X. Wu, N. Stanford, D.M. Fabijanic, Effect of hot isostatic pressing on the microstructure and mechanical properties of additive manufactured AlxCoCrFeNi high entropy alloys, Mater. Sci. Eng. A 733 (2018) 59–70.

[187] V. Ocelík, N. Janssen, S.N. Smith, J.T.M. De Hosson, Additive manufacturing of high-entropy alloys by laser processing, JOM 68 (2016) 1810–1818.

[188] M.S.K.K.Y. Nartu, T. Alam, S. Dasari, S.A. Mantri, S. Gorsse, H. Siller, N. Dahotre, R. Banerjee, Enhanced tensile yield strength in laser additively manufactured Al0.3CoCrFeNi high entropy alloy, Materialia 9 (2020).

[189] M. Li, J. Gazquez, A. Borisevich, R. Mishra, K.M. Flores, Evaluation of microstructure and mechanical property variations in AlxCoCrFeNi high entropy alloys produced by a high-throughput laser deposition method, Intermetallics 95 (2018) 110–118.

[190] S. Singh, N. Wanderka, B.S. Murty, U. Glatzel, J. Banhart, Decomposition in multi-component AlCoCrCuFeNi high-entropy alloy, Acta Mater. 59 (2011) 182–190.

[191] D. Karlsson, G. Ek, J. Cedervall, C. Zlotea, K.T. Møller, T.C. Hansen, J. Bednarčík, M. Paskevicius, M.H. Sørby, T.R. Jensen, U. Jansson, M. Sahlberg, Structure and hydrogenation properties of a HfNbTiVZr high-entropy alloy, Inorg. Chem. 57 (2018) 2103–2110.